Aline Wilm Senna Pinto

Estudo Numérico de Jatos Compressíveis em Escoamentos Cruzados

PROJETO DE GRADUAÇÃO

DEPARTAMENTO DE ENGENHARIA MECÂNICA
Programa de Graduação em Engenharia Mecânica

Rio de Janeiro
30 de Junho de 2016

Aline Wilm Senna Pinto

Estudo Numérico de Jatos Compressíveis em Escoamentos Cruzados

PROJETO DE GRADUAÇÃO

Projeto apresentado como requisito para obtenção de
grau de Bacharel pelo Programa de
Graduação em Engenharia Mecânica do
Departamento de Engenharia Mecânica da PUC-Rio.

Orientador
Professor Luís Fernando Figueira da Silva

Rio de Janeiro
30 de Junho de 2016

Aline Wilm Senna Pinto

Numerical Study on Compressible Jets in Crossflows

UNDERGRADUATION FINAL DESIGN PROJECT

MECHANICAL ENGINEERING DEPARTMENT
Mechanical Engineering Undergraduation Program

Rio de Janeiro
June 30th, 2016

Aline Wilm Senna Pinto

Numerical Study on Compressible Jets in Crossflows

UNDERGRADUATION FINAL DESIGN PROJECT

Project presented as a requirement for the acquisition of a Mechanical Engineering Bacharel Degree on the Mechanical Engineering Department from PUC-Rio.

Professor
Professor Luís Fernando Figueira da Silva

Rio de Janeiro
June 30th, 2016

List of Figures

List of Tables

Sumário

O presente relatório descreve um estudo numérico de jatos compressíveis em escoamentos transversais, que possui diversas aplicações na engenharia como injeção de combustível em câmaras de combustão e controle de manobras em veículos aeroespaciais. O domínio de simulação foi definido de forma similar à literatura e tem como objetivo reproduzir o ambiente onde jatos são expostos à escoamentos transversais. O programa *blockMesh* foi utilizado para a geração de malha, as simulações numéricas foram rodadas em paralelo através do *OpenFoam 3.0.0* e o pós-processamento feito com o *ParaView*. Além disso ainda foram realizadas uma extensa pesquisa biliográfica e uma análise dos resultados obtidos.

Abstract

This project describes a numerical study and analysis of compressible jets in crossflows, which has a wide field of engineering applications including fuel injection in combustion chambers and aerospace vehicles manoeuvring. The simulation's domain was defined in a similar way to the ones found in the literature and is supposed to reproduce the environment conditions where jets are exposed to crossflows. For the mesh generation *blockMesh* was used, the numerical simulations were run in parallel through an open-source program called *OpenFoam 3.0.0*, the post-processing data was done with *ParaView*. Besides that this report includes an extensive bibliographic research and comments on the results obtained.

Contents

1 Introduction

The aim of this work is to perform a numerical study of jets in crossflows, both in the supersonic flow regime. This flow configuration can be applied in the aerospace systems, such as for the injection of fuel on engine combustion chambers, cooling systems for high temperature engine parts, missiles or atmospheric re-entry vehicles that needs some kind of control mechanism for manoeuvring. In the case of engine applications, the efficient fuel mixing with air, as well as the accurate description of the flow field behaviour of this kind of arrangement is critical. Such description requires a detailed physical understanding of the supersonic fluid flow. Although data for incompressible jets in crossflows are easily found in the literature, some researchers have concentrated their attention for both numerical and experimental studies for higher Mach number fluid flows.

This specific topic has been chosen as the subject of this project because it is the continuity of a research experience I had in *University of Minnesota* in the *Aerospace and Mechanics Department* with professor Krishnan Mahesh in 2015. As I intend to pursue a masters degree and then a PhD on computational fluid dynamics area, this is a great opportunity to get deepen my understanding on physical properties and to practice with the tools and resources commonly used to perform such a study. Also, following previous opportunities I had, I felt compelled to work on a topic with aeronautical applications, specially this one, which is related to fuel injection and propulsion efficiency. Even though this work deals with simplified methods and configurations due to some technical restrictions faced during its development, it allows for deepening and widening my knowledge understanding on numerical simulations and compressible flows.

The studied configuration is a jet flow that interacts with a transverse surrounding flow. In this work a simplified version of such a classical configuration of jets in crossflows is of interest so that general fluid flow behaviour and compressible supersonic flow parameters could be observed and analysed. The simulation domain consists of a rectangular box for the free-stream flow attached to a convergent nozzle and the domain dimensions have been chosen according to previous researches. The meshes were generated through an *OpenFoam* utility called *blockMesh* and simulations were run in parallel using *OpenFoam 3.0.1*. To post-process the data, a software called *ParaView was used*.

This report starts with a brief literature review and identifies the key parameters and features that are usually observed in this particularly fluid flow configuration. Then the mathematical formulation is presented and the key elements of the theory of compressible fluid flow required to the understanding of physical phenomenons are discussed in latter chapters. The third part consists on the methodology section, where the resources, schemes, configuration setting, meshing generation and boundary conditions are described. Finally, the results are present followed by a brief conclusion of the work.

The articles and books used in this work are listed in the references and the majority of them were extensively studied to compose the scientific content of this project. An special attention was given to the works from: *K. Mahesh*, *D. Peterson*, *J. D. Holdeman* and the computational fluid dynamics book from *K. A. Hoffmann and S. T. Chiang*.

2 Objectives

The general objective of this work is to undertake a numerical study of compressible jets issuing in a cross flow in situations representative of aerospace applications.

The specific objectives of this work are:

- To perform a literature review in order to understand the historical background of such configuration and to identify the parameters and concepts needed to deal with jets in cross flows and compressible fluid flow.

- To learn how to generate both 2D and 3D meshes for the studied configuration, which involve determining the suitable tools to create the grids and how to prescribe the desired mesh parameters had to be set.

- To explore *OpenFoam* and its extensions for solving a supersonic compressible flow problem.

- To perform preliminary tests so as to ensure proper the configuration of the problem studied, in particular, to investigate parallel processing efficiency and boundary conditions influence.

- To study the behaviour of to dimensional compressible jets in the absence and in the presence of cross flow.

- To pave the way for more ambitious three-dimensional configuration studies.

3 Literature Review

Jets in crossflows have been studied for more than 60 years. However, this field of study is far from fully explored. Indeed, as the methodologies and resources applied for the numerical simulations and experimental sets become more sophisticated, flow features and behaviour may be better characterized and understood.

This chapter describes the main findings in jet interaction with transverse flows and details the historical background of this study.

3.1 Experimental Studies

The first observations of fluid flow behaviour were performed by means of experimental studies. Until nowadays such studies are used to validate numerical simulations, set the basic theoretical definitions and to help better understand the physical phenomena that characterizes the flow nature. In this section a review of experimental data and methods is presented with an intention to summarize the knowledge evolution in such an area.

Kamotani and Greber [27] were among the first researches to perform experimental studies on JICS (Jets in cross flows). They used hot wire anemometers and thermocouples to measure flow field properties of heated and unheated round turbulent jets. They demonstrated that jet velocity and temperature trajectories are mainly determined by the momentum ratio and that a pair of vortices forms downstream the jet immediately after exiting from the nozzle. Other vortex structures are also formed. Also, they observed that the turbulence intensity increases with increasing momentum ratio. *Isaac et al.* [24], *Menon and Gollahali* [38] and *Sherif and Pletcer* [50] also used hot wire anemometers and thermocouples for measurements on flows with velocity ratios ranging from 2 - 6 and jets separation distances of 8, 12 and 16D.

More recently, other works were performed with more accurate flow measurement techniques such as PIV (*particle image velocimetry*). *Holdeman* [22], *Clemens and Mungal* [8] and *Ccacya and Figueira da Silva* [5] used this technique to study situations with variations in momentum-flux ratio and orifice size and spacing, which have been found to have a significant effect on the

flow structure. Also, the jet structure was observed to be slightly different for jets injected in different axial directions. These experiments were performed for velocity ratios of 0.5, 1 and 1.5 with jet spacing-to-jet ratio of 3 and free stream Mach numbers of $0.28, 0.42, 0.5, 0.62$ and 0.79. The obtained results suggest that compressibility increases the amount of momentum, thus improving the molecular mixing efficiency even though previous studies have shown the opposite. *Ajersch et al.* [1] used laser Doppler velocimeters and smoke generators to observe the fluid field.

Hasselbrink and Mungal [19], *Ben-Yakar et al.* [3] and *Ccacya and Figueira da Silva* [5] used OH-PLIF (*OH Planar Laser Induced Fluorescence*) to analyse more complex configurations like in supersonic regimes or reactive flow fields. The results show that: the momentum flux ratio is the main controlling parameter of the jet penetration; extra forces act on the vortex structure and also that the flame/flow interaction that was found to be stronger near the jet orifice.

Johari et al. [25], *Han and Mungal* [17], *Ibrahim and Gutmark* [23], *Kolar et al.* [31] and *Naik et al.* [41] combined the results obtained with PIV and hot film anemometers. However this can be explained by the level of complexibility of their experimental set-ups: Those fluid fields had velocity ratios of 1, 2 and 4 and a maximum $\triangle T = 300K$.

Observations taken from the most recent works from *Peterson and Candler* and *Chai, Iyer and Mahesh* allow to conclude that vorticity and jet penetration are strongly dependant on geometrical parameters, such as jet spacing, orifice format and angle of incident into the free stream flow. Remarks on the heat release of the jet were pointed: they have dominant effect on entrainment.

3.2 Numerical Studies

The numerical studies performed for JICS first began with RANS (Reynolds Averaged Navier Stokes) simulations, then progressed to DNS (Direct numerical simulations), LES (Large-eddy simulations) and finally a mixed method called hybrid RANS-LES. A brief description of each turbulence model will be given in section 4.3, page 16. *Holdeman* [22], *Demuren* [10] and *Kim and Benson* [30] modeled subsonic jets interaction with crossflows using RANS based on a finite volume method. They determined that the fluid flow of a row of jets in a confined crossflow is a

highly complex flow that includes unsteady vortex systems located in the wake and side regions of the jet and a horseshoe vortex structure along the surroundings of the jet exit. A comparison of their results allows to conclude that trajectories corresponding to round and rectangular orifices are similar if their jet-to-mainstream momentum-flux and orifice-spacing are equal.

Ajersch et al. [1] used $k-\varepsilon$ turbulence model for simulating isothermal JICS with velocity ratios of 0.5, 1 and 1.5 and jet spacing ratio of 3.

Sau, Muppidi and Mahesh [47] [39] used DNS to study JICS cases for round turbulent jets in a laminar crossflow with a velocity ratio between the jet and the free stream flow of 5.7 and $Re_D = 5000$. To capture near-wall scales and the effect of crossflow on the dynamics, entrainment and mixing characteristics on the vortex structures, those simulations demanded high computational costs due to the use of a DNS. It was concluded that, for a velocity ratio smaller than 2, complete vortex structures are not formed.

Kawai and Lele [29] usde LES to characterize a challenging ase, i.e., a fluid flow with a free stream Mach number of 1.6, $Re_D = 2.4x10^4$, density ratio and pressure ratio between the jet and the crossflow of 5.55 and 8.4 respectively and a momentum flux ratio of 1.7. Those conditions have been experimentaly studied by *Santiago and Duton* [46] in 1997. *Kawai and Lele* [29] observed that the flow field was highly unstable with repeated large-scale deformation of shock and vortex structures. Pressure fluctuations within the recirculation region were found to be coupled with both barrel and bow shocks accompanied by large-scale vortex formation in the windward jet boundary.

A hybrid RANS-LES method was used by *Higgins and Schmidt* [20] and *Peterson and Candler* [43]. Large scale unsteady structures were captured by the LES, whereas RANS was used in the wall regions to capture the turbulent scales. This approach reduces the overall computational requirements, since the grid should be only refined near the wall region. The flow field main parameters were the same from *Kawai and Lele* [29], based on *Santiago and Duton* [46] experiments. Their simulations showed that the jet blocks the crossflows, producing a 3D bow shock. Furthermore, a small recirculation region emerged upstream the jet, due to a separation of the approaching crossflow boundary layer. Downstream the orifice, the jet expands before being compressed by a

barrel shock and a Mach disk. The jet is then observed to bend towards the direction of the main crossflow becoming dominated by a CVP. Also, it was found that the lower momentum flux ratio cases had the highest levels of mixing efficiency.

Doom, Hou, Chai and Mahesh [6] [11] used both DNS and LES methods to simulate compressible turbulent reacting non-dissipative flows based on experiments from *Santiago and Duton* [46]. A reasonable agreement was observed with the experimental data and their work showed optimistic chances to reproduce complex flow through an unstructured algorithm that they developed.

3.3 Theoretical Studies

Hasselbrink and Mungal [18] and *Soo-Young No* [52] developed theoretical analysis of JICS (jets in cross flows) phenomena descriptions. These authors present a similarity analysis, which is a summary of the jet scaling ideas adopted in some experiments. Their approach demonstrated that, in the vicinity of the jet exit, the axial jet velocity is r (velocity ratio) times larger, and is changing r times faster, than the crossflow component of velocity. Also, they analysed some empirical correlations for jet penetration from the literature and compared them to theoretical concepts and experimental results.

3.4 Jets in Compressible Crossflows

Jets in crossflows comprises an interaction between a main flow and a flow issuing from an orifice. To describe the instantaneous behaviour, the literature commonly refers to some quantitative terms that are described below, together with some qualitative characteristics of the flow.

3.4.1 Quantitative Description

The interaction of jets in supersonic crossflows results in a complex 3D flow field . The most basic description of the flow is that of the jet trajectory, also known as the penetration depth in the free-stream flow.

Jet Trajectory

The jet trajectory describes how far the transverse flow penetrates into the main surrounding flow. It is usually measured as the height between the orifice exit plane and the point where the chosen jet trajectory criteria is found along the domain of interest. The trajectory may be defined as the path formed by many parameters such as: positions of maximum local velocity, local maximum scalar, maximum vorticity, etc. Therefore the trajectory may change subject to the chosen parameter. For supersonic jets and crosflows, jet penetration depends on the momentum flux ratio and the following terms (pressure, density, temperature, molecular weights and Mach number ratios),i.e.,

$$\frac{p_{jet}}{p_\infty}; \frac{\rho_{jet}}{\rho_\infty}; \frac{T_{jet}}{T_\infty}; \frac{W_{jet}}{W_\infty}; \frac{M_{jet}}{M_\infty}. \tag{1}$$

Empirical correlations for jet trajectories may be based on visualization of the flow, and relates some of the ratios above to the penetration depth of the jet scaled with the orifice diameter.

The momentum ratio for supersonic flows is considered to be the controlling parameter to describe the jet trajectory, and is present in the majority empirical correlations found in the literature,

$$J = \frac{\gamma_{jet}}{\gamma_\infty}\frac{p_{jet}}{p_{\infty 2}}M_{jet}^2\frac{2\gamma_\infty}{\gamma_\infty+1} - \frac{\gamma_\infty - 1}{M_\infty^2(\gamma_\infty+1)}. \tag{2}$$

Where γ is the rate of specific heats, M is the Mach number and the subscripts ∞, $\infty 2$ and *jet* refer to the surrounding fluid flow, after bow shock fluid flow and jet flow respectively.

Schetz and Billig [48] introduced one of the first empirical correlations and further continued to explore supersonic crossflows adding many contributions to the area. These authors used the Mach disk height as a measure of jet penetration and considered the forces acting on the fluid away from the shock waves.

McDaniel & Graves (1988), *Rothstein & Wantuck* (1992), P*apamoschou & Hubbard* (1993), *Gruber et al.* (1997) and most recently, from *Beresh, Henfling, Erven and Spillers* (2005) and *Chai, Iyer and Mahesh* (2015), either proposed new correlations or suggested slight changes in previous studies to improve their accuracy. Some of the correlations with different dominant

parameters considered, written in the power law form ($\frac{y}{Jd} = aJ^b \left(\frac{x}{Jd}\right)^c$).

$$\frac{y}{dJ} = 1.2\left(\frac{x+d/2}{dJ}\right)^{0.344}, \tag{3}$$

$$\frac{y}{d} = 2.173J^{0.276}\left(x/d\right)^{0.281}, \tag{4}$$

$$\frac{y}{d} = \frac{0.344}{M_\infty^2}\frac{p_j}{p_\infty} ln\left[2.077\left(x/d + 2.059\right)\right]. \tag{5}$$

3.4.2 Flow Field Structure

The qualitative behaviour of the flow field structure is available in the literature due to both experimental and numerical studies. To capture fluid flow structure and characteristics, the pioneering experimental works used hot wires and laser Doppler anemometry, triple wire probes, hot films, whereas the most recent employed smoke illuminated by lasers, hydrogen bubbles, PIV (Particle Image Velocimetry) and PLIF (Planar Laser-Induced Fluorescence). Regarding the computational studies, the methods progressed from RANS to DNS, LES and RANS-LES hybrid simulations, where large-scale unsteady structures are captured by LES and near the walls, RANS is used. This method reduces the overall mesh resolution requirements, thus optimizing the computational costs. More details about the historical background are included in section 3, on page 4.

Before analysing the flow structure, it is important to define some specific terms that will be required such as *CVP* and *horseshoe vortex*.

- **CVP**

  The flow structure known as *counter-rotating vortex pairs*, *CVP* are unsteady and instantaneously asymmetric features. It is initiated at the near-field of the jet orifice exit due to pressure gradients caused by the jet obstruction and such a structure develops along the flow. Figure 1 shows several time-averaged cross sectional views of a jet issuing in a crossflow.

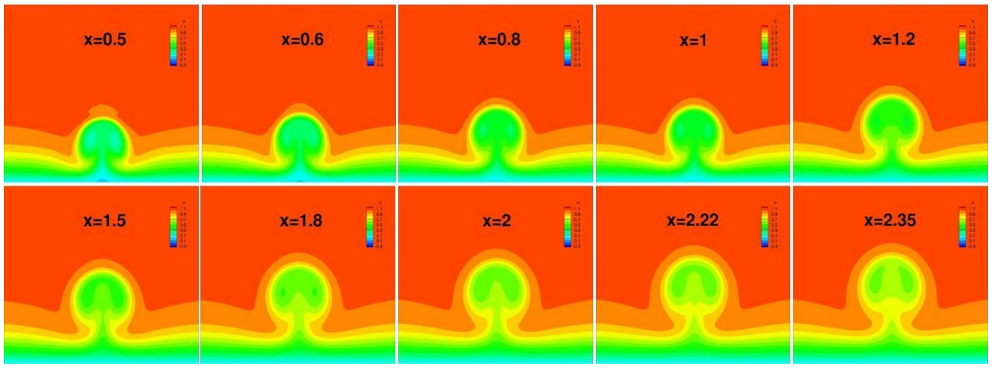

Figure 1: CVP formation along the stream-wise direction.

- **Horseshoe vortex**

  Horseshoe vortexes are formed immediately downstream the jet's exit, due to the crossflow boundary layer interaction with an adverse pressure gradient. Those vortices are periodic and move around the jet. Depending on the velocity of the jet and the free stream flow, they may be either steady or oscillatory. Both *CVP* and *horseshoe* vortices can interact, merging one into the other.

Similarly to incompressible jets in crossflows, the instantaneous flow field behaviour consists of a complex structure of vortexes and recirculation zones. In the supersonic regime, the upstream turbulent/laminar boundary layer from the free stream flow decelerates and separates in response to the jet forming a bow shock and horseshoe vortex. In this separated region a pressure gradient in the stream wise direction is established as well as vorticity of different signs making the jet flow bends in the same way. When the flow is analysed on a time-averaged manner, a CVP vortex structure can be seen. Beneath the bow shock, the jet flow penetrates and expands into the crossflow, forming a barrel shock. Small recirculation regions may be observed immediately upstream the jet exit due to the boundary layer separation. The jet flow is then compressed by a Mach disk. Figure 2 shows an schematic version of the phenomenons described above.

The jet plume was found to exhibit unsteady behaviour by *D. Peterson* [43] and *K. Higgins* [20]. The unsteadiness is believed to be related to acoustic wave propagation and the high-speed flow exiting the jet orifice. Figure 3 shows a 3D simulation instantaneous capture that

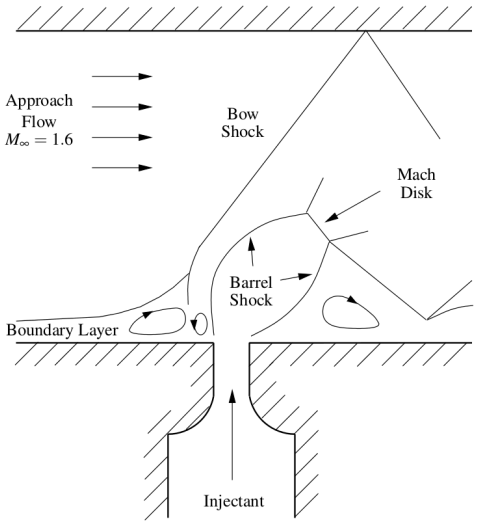

Figure 2: Two-dimension scheme of a jet interaction with a supersonic crossflow. Picture taken from *Higgins and Schmidt, 2007* [20].

illustrates all the terms that quantitatively characterizes supersonic jets in crossflows.

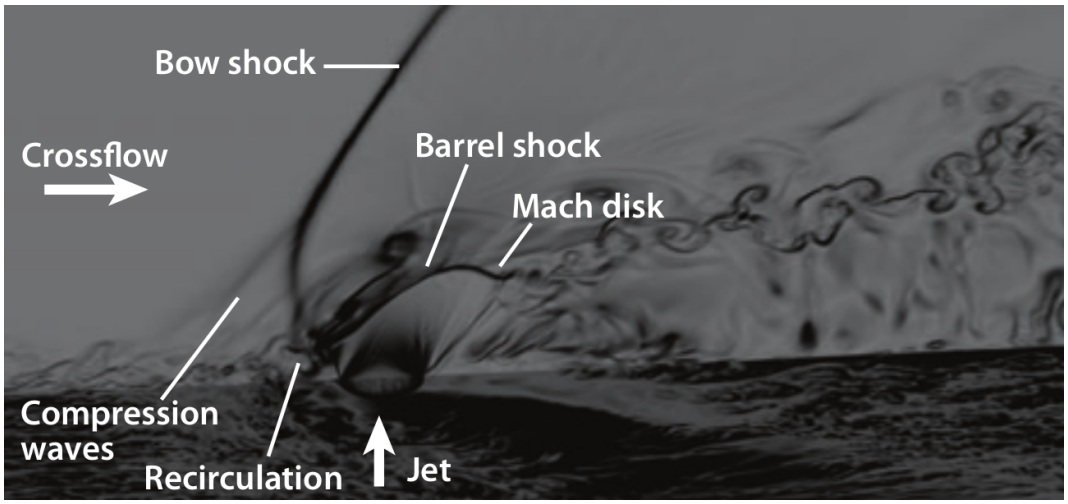

Figure 3: Three dimensional view of instantaneous qualitative behaviour of density gradient magnitude contours. Picture taken from *Chai and Mahesh, 2011* [6].

4 Mathematical Formulation

4.1 Conservation Laws

Conservation of Mass

The conservation of mass theory is one of the most important governing principles in fluid mechanics and it states that mass is neither created nor destroyed. In fluid mechanics, for a finite volume control, the total mass in steady state should always be constant. The conservation of mass also known as the continuity equation, can be written in the differential form as:

$$\frac{D\rho}{Dt} \equiv \frac{\partial \rho}{\partial t} + \mathbf{u} \cdot \nabla \rho \equiv \frac{\partial \rho}{\partial t} + \frac{\partial}{\partial x_i}(\rho u_i) = 0 \tag{6}$$

Conservation of Momentum

The conservation of momentum is the expression of the Newton's second law $\left(\overrightarrow{F} = \frac{d(m\overrightarrow{v})}{dt}\right)$ that states the sum of the forces is equal to the rate of change of momentum in an inertial frame. There are two kind of forces that a fluid element can experience: Surface forces (pressure and shear stresses for instance) and body forces (usually due to gravity). The momentum conservation equation is derived by considering a fluid element, as shown inf figure 4.

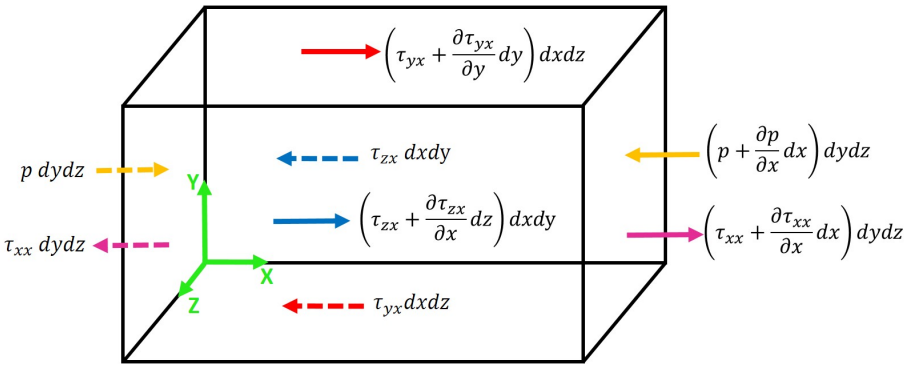

Figure 4: Elementary control volume and forces acting on it.

These equations, also known as the Navier-Stokes equations are given by:

$$\rho \frac{Du_i}{Dt} = -\frac{\partial p}{\partial x_i} + \left(\frac{\partial \tau_{ii}}{\partial x_i} + \frac{\partial \tau_{ij}}{\partial x_j} + \frac{\partial \tau_{ki}}{\partial x_k} \right) + \rho f_i \tag{7}$$

Another way to write this equation is:

$$\frac{\partial \overrightarrow{V}}{\partial t} + \left(\overrightarrow{V} \cdot \nabla \right) \overrightarrow{V} - \upsilon \nabla^2 \overrightarrow{V} = -\frac{\nabla p}{\rho} + \overrightarrow{g} \tag{8}$$

Energy Conservation

From the first law of thermodynamics $\left(\dot{Q} + \dot{W} = \left(\frac{dE}{dt} \right)_{system} \right)$, the conservation of energy states that it means that the rate of change of total energy of a system must be equal to the input of mechanical and thermodynamic energy fluxes.

$$\left\langle \rho \frac{De}{Dt} \right\rangle_{thermo} + \left\langle \rho \frac{DK}{Dt} \right\rangle_{mech} = \langle -\nabla \cdot \mathbf{q} + \rho r \rangle_{thermo} + \langle \nabla \cdot (\boldsymbol{\text{œ}} \cdot \mathbf{U}) + \rho \mathbf{g} \cdot \mathbf{U} \rangle_{mech} \tag{9}$$

Alternately, the equation above can be written in an Index form (equation 10), that is very common in the literature.

$$\frac{\partial}{\partial x_i} = \left(-p \frac{\partial u_j}{\partial x_j} + \sigma_{ij} \frac{\partial u_j}{\partial x_i} \right) + \left(-u_j \frac{\partial p}{\partial x_j} + u_j \frac{\partial \sigma_{ij}}{\partial x_i} \right) \tag{10}$$

Where the terms represent the pressure and viscous stresses that lead to the deformation of the fluid element and some other factors that can either increase or decrease the fluid kinetic energy. If equation 10 is further expanded, it is possible to identify some terms as pressure diffusion, turbulent transport, molecular viscous transport, production and dissipation of energy in the form of eddies and buoyancy flux.

Rearranging the energy conservation equation, the total energy can also be defined as 11 that is the exact equation calculated by the solver, according to the methods selected.

$$\frac{\partial \rho E}{\partial t} + \nabla \cdot (\rho \mathbf{U} E) + \nabla \cdot (\mathbf{U} p) = -\nabla \cdot \mathbf{q} + \nabla \cdot (\boldsymbol{\text{ø}} \cdot \mathbf{U}) + \rho r + \rho \mathbf{g} \cdot \mathbf{U} \tag{11}$$

4.2 Compressible Flows Overview

4.2.1 Basic concepts

Compressible flows involves density variations coupled with the pressure field. Often, the fluid velocities are comparable to the velocity of sound and the variations in pressure, temperature and density are important to describe the flow dynamics. Compressible flows behaviour is significantly different when compared to incompressible flows.

4.2.2 Normal and Oblique Shock Waves

Under some circumstances, spontaneous discontinuities in pressure, temperature, density and velocity may occur in a flow. The thin region over which such sharp changes happen is also named *shock waves*. Figure 5 illustrates typical properties change when such waves occur.

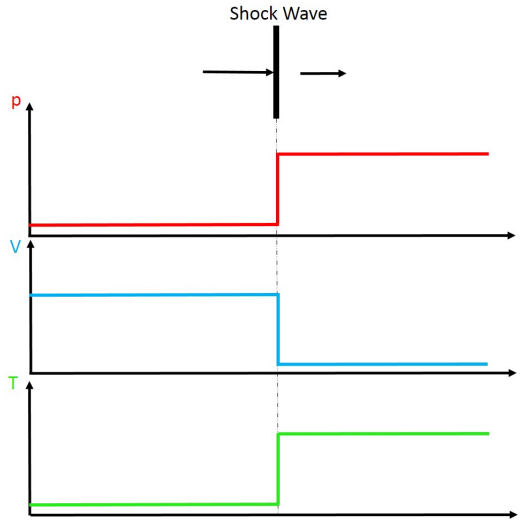

Figure 5: Changes in pressure, velocity and temperature as a shock wave propagates.

A normal shock wave happens when a source is travelling at a higher speed then its propagation rate and the elements in front of the source do not interfere on the downward fluid flow because it does not notice the coming information. As the name implies, a normal shock wave is a straight finite region perpendicular to the surface that creates discontinuities in the flow.

Oblique shock waves are somehow similar to normal shock waves with an exception to its inclination/deflection relative to the wall. When a fluid element goes through an oblique shock,

it suffers some discontinuities and slightly changes its movement direction.

4.2.3 Mach Cone

The Mach cone is an important phenomenon in wave propagation that happens when the source is travelling faster than the propagation speed. Figure 6 illustrates the wave propagation for sources travelling at the same and faster speeds of sound. This can explain why in supersonic cases, the boundary conditions do not imply unknown information from the environment outside the simulation's domain.

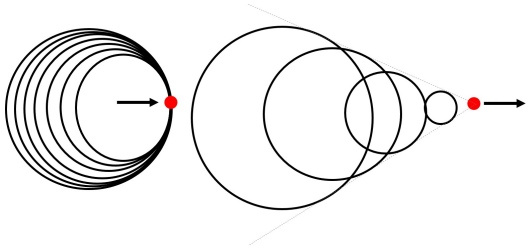

Figure 6: Wave behaviour for a source travelling at the same (left) and higher propagation speed (right).

4.2.4 Nozzles

Because the jet goes through a nozzle before it interacts with the crossflow, it is important to understand be basic concepts about convergent and divergent nozzles. For subsonic flows, an increasing cross-sectional area (divergent nozzle) implies a decrease in velocity whereas convergent nozzles make the fluid flow to accelerate. The exact opposite behaviour occurs for supersonic flows. However, for both subsonic and supersonic regimes, Mach 1 (sonic condition) at the throat (the smaller cross-sectional area with $dA = 0$) can occur, although it is not required.

A relationship between the local static pressure, temperature, density and cross-sectional area for isentropic flows is given by equation 12.

$$\frac{A}{A^*} = \left(\frac{2}{\gamma+1}\right)^{(\gamma+1)/[2(\gamma-1)]} \sqrt{\frac{\gamma-1}{2}} \left(\frac{p_0}{p}\right)^{1/\gamma} \frac{1}{\sqrt{1-\left(\frac{p_0}{p}\right)^{(\gamma-1)/\gamma}}} \tag{12}$$

From this equation, it is possible to establish the pressure at the nozzle inlet, its cross-sectional area and also predict some other parameters in the simulation's domain.

4.3 Fluid Flow Turbulence

The majority of flows encountered in engineering practice are turbulent and therefore require different numerical modelling methods so specific vortex and energy dissipation scales may be properly solved. They are characterized by its highly unsteady flow field, great vorticity and energy propagation between elements. In this section a brief description of some available turbulence modeling methods is presented. A description of those approaches goes beyond the scope of this report.

4.3.1 RANS

Reynolds-averaged Navier-Stokes equations are the result of the Reynolds decomposition on the Navier-Stokes equations that basically divides the equations in both time-averaged and instantaneous turbulence terms, also known as fluctuating parameters. This approach cannot represent turbulent unsteady features of the flow field and is mainly used to compute the Reynolds stresses. This method is characterized by different turbulence models that involves the approaches: *Linear eddy viscosity models*, *Nonlinear eddy viscosity models* and *Reynolds stress model*.

4.3.2 DNS

Direct numerical simulations (DNS) is the most accurate approach to turbulent simulation because it solves the Navier-Stokes equations without any kind of averaging or approximations, where all the motions contained in the flow are resolved. This method permits an easier error control and is the closest approach to laboratory experiments.

To assure that all the significant structures are captured, the spatial separation of sampling points should not be greater than the Kolmogorov microscale (from the energy scale theory):

$$\eta = \triangle x = Re^{-3/4} l \tag{13}$$

When *Re* is large, DNS requires a very fine grid to properly compute all turbulent eddies. Therefore, this is a high computational cost method but because of it accuracy, it is still used by some researchers.

4.3.3 LES

Large eddy simulation is another turbulence modeling method that nowadays is used by a significant number of people. In this approach, large eddies are more exactly treated than smaller ones because small eddies are much weaker and provide little disturbance or effect on fluid flow properties. Because of this approximation, LES is a much cheaper method than DNS that permits the user to solve complex simulations with high Reynolds numbers.

LES filters off smaller eddies and solves the Navier-Stokes equations for the bigger scale structures. For the eddies that were at first unconsidered, a modeling approximation is done, that is also known as the *subgrid-scale* model.

4.3.4 Hybrid RANS-LES

Hybrid RANS-LES simulations are usually used on applications that require a very accurate capture of unsteady features and scales of a flowfield. On critical parts of the domain such as near the walls where the flow is attached, RANS method is used to solve mean flow quantities while LES captures large-scale unsteady structures.

4.4 Numerical Solver

The solver used in this work is called *rhoCentralDyMFoam* that is a density-based compressible solver based on central-upwind schemes of Kurganov and Tadmor. The solver goes through each governing equation separately: It first solves the continuity equation (finding a new ρ), then it solves the momentum equation (both viscid and inviscid parts) and finally the energy equation is solved. The temperature is calculated after the energy-balance equation and the pressure is updated by the law $p = \rho RT$. Kurganov and Tadmor is a second-order high-resolution default scheme used in OpenFoam to solve compressible fluid flow problems. Kurganov and Tadmor uses *monotone*

upwind schemes for conservation laws (MUSCL) that is a finite volume method of higher order that can provide reasonable results for fluid flows with discontinuities (shocks) or large gradients caused by the high Mach number characteristics of the flow. More details can be found in [33].

5 Methodology

5.1 Resources

To perform the simulations of this work, the open source CFD C++ software *OpenFOAM 3.0.1* has been used. This software has been chosen due to its flexibility, i.e., the different available solver options, the various online support forums and the lack of any licensing or fees. Furthermore, it allows for a certain awareness and manipulation capabilities of the methods and approaches used to perform the simulations. Its extensive range of features intends to allow, in particular, the solution of complex high speed fluid flows providing turbulence models and even the possibility of considering reacting mixtures. A detailed step by step set-up procedure is given below since the first contact with *OpenFoam* occurred during this work.

The procedure of setting the inputs for physical and fluid properties, initial and boundary conditions to perform an analysis is called **pre-processing**. The information provided to the code is spread in three main directories: *0*, *constant* and *system*. This is an interesting feature from *OpenFoam*, since one can easily access and check the properties of the simulations and analyse log reports in text formats.

Figure 7 shows an schematic tree of a case structure in *OpenFoam*:

- ***0* directory**

  In the *0* directory, the user sets the boundaries, internal fields, dimension units and initial conditions of the case $(t = 0s)$. Depending on the solver choice some particular extra parameters must be defined, otherwise only *pressure*, *temperature* and *velocity* fields should be given initial conditions.

- ***constant* directory**

  In the *constant* directory there are found the mesh data and the physical transport and turbulence specifications files. For most solvers, the *turbulenceProperties* file determines the turbulent model used (*RANS*, *LES*, *laminar*, etc). On the *thermophysicalProperties* file, thermodynamic properties of the fluid are specified. In the particular case of the solver used in

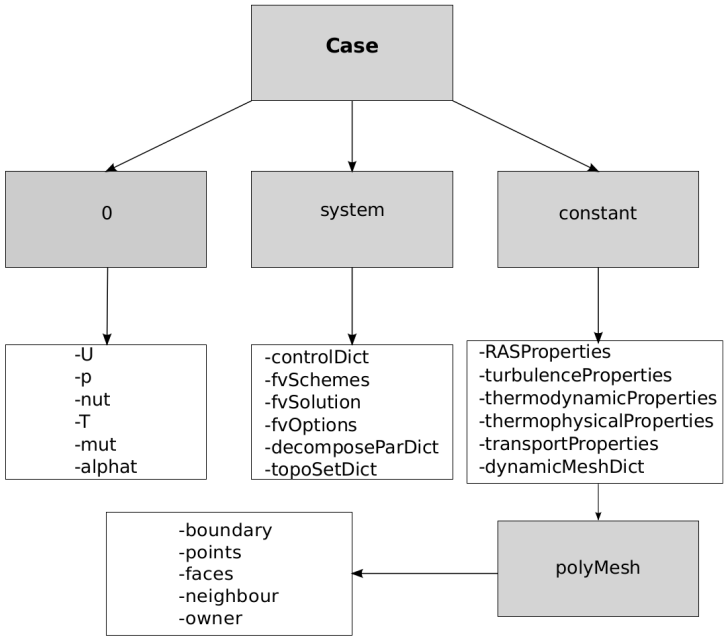

Figure 7: Systematic representation of an *OpenFoam's* case set-up. Picture taken from *Magnus Winter* [35].

this project (*rhoCentralDyMFoam*), there is another file in the *constant* directory, *dynamicMeshDict*, that could allow to perform simulations with moving meshes.

- ***system* directory**

  In the *system* folder, are found the files that contain the simulation specifications. In the *controlDict* dictionary, some items such as the simulation's runtime, *Courant* number, output files options are assigned. In *fvSchemes* the numerical methods and schemes of the simulation are specified and in the *fvSolution* dictionary, the solver and its tolerances are assigned.

The **mesh generation** has been performed was done using an utility supplied with *OpenFOAM*,*blockMesh*. The simulation domain should be decomposed into hexahedral blocks. Besides defining the coordinates of each vertice and which edges compose the faces of the blocks, it is also can also required to specify the number of cells in each direction and the corresponding expansion ratios. The mesh configuration is read from a dictionary named *blockMeshDict* and *blockMesh* reads the file and writes out the mesh data in many different files describing the information of the vertices, faces, cells and boundaries. To **process** the mesh data, a pre-programmed solver called

rhoCentralDyMFoam was used to do all the mathematical calculations of the specified conditions.

To **post-process** the data generated by the solver, a software called *ParaView* was used. It is a data analysis program that allows the user to use both qualitative and quantitative methods to observe the results of the simulation. The main features used were glyphs, streamlines, contours, isosurfaces, plots in function of time, wireframe view of the mesh and animation tools.

5.2 Parallel Processing

The simulations performed in this work were run in parallel, using an *OpenFoam's* utility called *decomposePar*. This method is based on a *simple* domain decomposition, in which the geometry is automatically broken into parts allocated to each processor. This division is made so that each processor has approximately the same number of elements to solve.

In most CFD studies, simulations are run in parallel to reduce computational costs and accelerate the calculation process. However, a good balance between the number of processors used and the amount of elements assigned to each of them should be established otherwise the "communication" effort between processors could negatively impact the CPU time. The determination of the optimal elements number each processor should be assigned without slowing down the simulation is shown in section 6.1.1, page 35.

Although parallel processing was adopted, the mesh used (thus the results resolution) in the present report is constrained by a computational capability restriction: The simulations were run in a Intel® Core™ i7 with 8 processors @ 2.50GHz with 378.8 GB disk space. A comparison of the grid refinement between the mesh created in this work and other simulations from the literature may be found in table 3, page 31.

5.3 Schemes

5.3.1 Interpolation Scheme

The interpolation scheme terms are written in the *interpolationSchemes* sub-dictionary and specifies the algorithms for point-to-point interpolations of values. For the present work, most interpo-

lations are made through a central differencing approximation, in exception for the ones specified below.

Density and Temperature Interpolation Schemes

For both scalar and vector fields such as temperature, density and velocity, an enhanced version of interpolation scheme is used. It is called TVD (Total Variation Diminishing) and uses a van Leer limiter. The TVD scheme can predict shocks without any misleading oscillations when there are discontinuities in the flow field parameters. And because of that, this scheme works well in coarser grids. The van Leer limiter can also be called flux limiter or slope limiter: They avoid unwanted oscillations and instabilities due to shocks in the solution domain.

5.3.2 Time Scheme

In the *ddtSchemes* sub-dictionary the first time derivative method is specified with Euler scheme, which is a first order and implicit approximation. For this method, the first-order wave equation 14 is rearranged as (6.13), where a is a constant positive speed. This is a commonly used technique to solve hyperbolic equations in inviscid supersonic flow fields.

$$\frac{\partial u}{\partial t} = -a\frac{\partial u}{\partial x} \tag{14}$$

$$\frac{u_i^{n+1} - u_i^n}{\triangle t} = -a\frac{u_i^{n+1} - u_{i-1}^{n+1}}{\triangle x} \tag{15}$$

5.3.3 Gradient and Divergent Schemes

The method chosen for the gradient and divergent schemes, on the *gradScheme* and *divScheme* sub-dictionaries was Gauss scheme, that is a standard second order, finite volume discretisation of Gaussian integration (equation 16). The Gauss linear method for calculating the gradient is very accurate on hexahedral meshes.

$$\int_{V_P} \nabla \phi dV = \oint_{\partial V_P} ds\phi = \sum_f \mathbf{s}_f \phi_f \tag{16}$$

The approximation of surface integrals requires knowledge of variables at the midpoints of the cell faces. As they are not part of the grid, an interpolation is needed. In this formulation, a linear interpolation of values are made from two neighbouring grid points: from cell centres to face centres (equation 17), where $f_x = \overline{fN}/\overline{PN}$ is the interpolation factor.

$$\phi_f = f_x \phi_P + (1 - f_x)\, \phi_N \tag{17}$$

For the surface normal gradient schemes, that are found in the *snGradSchemes* sub-dictionary, an explicit non-orthogonal correction evaluated at a cell face is applied.

5.3.4 Laplacian Scheme

Also known as the diffusion scheme, the Laplacian scheme is written in the sub-dictionary *laplacianSchemes* and the method chosen was the Gauss linear corrected. Similarly to the gradient and divergent schemes, the laplacian one is a gauss linear approximation with the slight difference that it has a corrected surface normal gradient scheme. It has a factor Γ that turns it conservative:

$$\int_{V_P} \Gamma \nabla \phi dV = \oint_{\partial V_P} ds\Gamma\phi = \sum_f \mathbf{s}_f \Gamma \phi_f \tag{18}$$

5.4 Boundary Conditions

In this section, a description of each boundary condition used on the simulations of this work will be given. Setting the boundary conditions is one of the most important steps of a simulation's because the fluid flow will respond in accordance to the inputs given by the user. If a boundary condition is posed in a wrong way, undesirable and non-physical results will appear.

In the present work, the domain was divided into 6 main surfaces: (1) Free stream flow inlet, *(2)* Nozzle inlet, *(3)* Free stream flow outlet, *(4)* Side walls, *(5)* Upper and bottom free stream walls and *(6)* Nozzle walls. Figure 8 illustrates those surfaces for a three-dimensionall grid. For

the two-dimensional domains, a similar division was made.

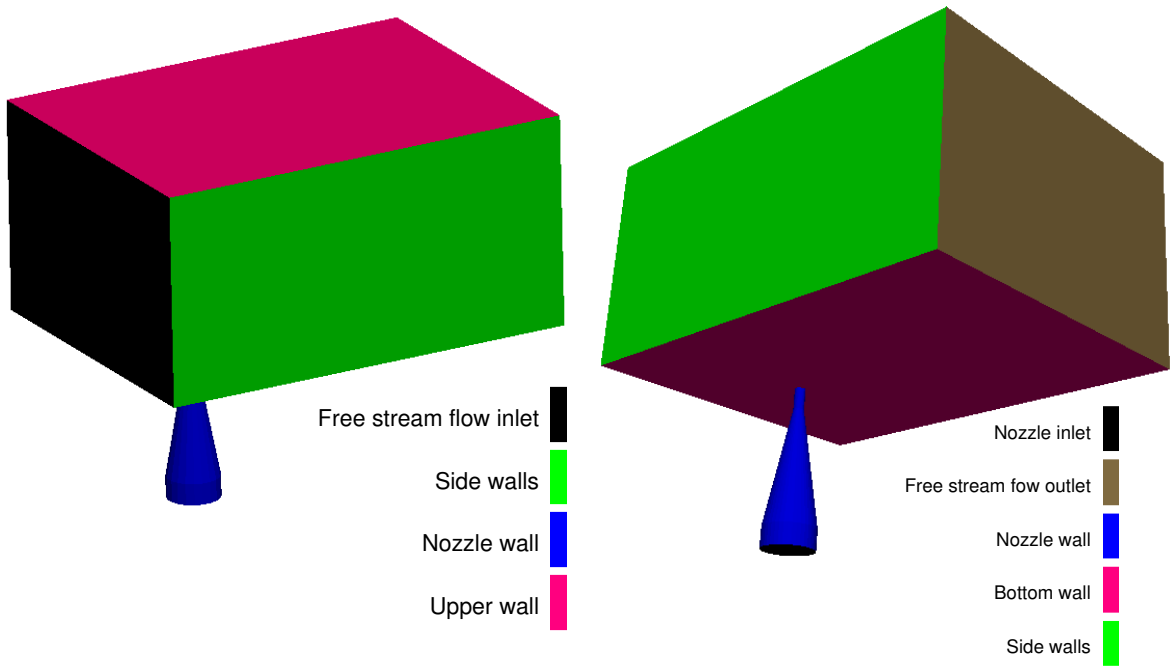

Figure 8: Boundary surfaces for a three-dimensional grid.

Before setting the cases and running the simulations, a brief research on the physical meaning of each boundary condition was made because the understanding of the flow inputs helps the interpretation of the results obtained.

- ***zeroGradient***

  In numerical studies, a zero-gradient boundary condition means that the derivative of a specific parameter is equal to zero. In other words, a backward difference approximation is made for the derivatives, as shown in equation 19:

$$\frac{\partial u}{\partial x} = \frac{u_i - u_{i-1}}{2} = 0 \Rightarrow u_i = u_{i-1} \tag{19}$$

  In OpenFOAM, this boundary condition can be given to all the parameters (velocity, pressure and temperature) by typing:

```
patch name { type        zeroGradient; }
```

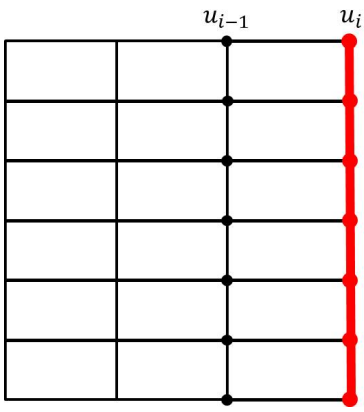

Figure 9: Numerical meaning of a zero-gradient boundary condition.

- ***fixedValue***

  For this boundary condition, a value is specified for a surface and it does not change at any time during the simulation. In other words, a constant value is fixed in the surface. This boundary condition is good for when you need to assure a value for the boundaries, letting other parameters adapt themselves to the fluid flow. This condition can be given to any parameter and should be written as:

```
patch name { type      fixedValue;
             value     300; }
```

- ***flowRateInletVelocity***

  This boundary condition is commonly used on inlet surfaces and it specifies the mass flow rate [kg/s] in the direction of the normal vector to the surface at which the fluid flow enters the simulation domain. This condition is only given in the *velocity* sub-dictionary and should be written as:

```
patch name { type      flowRateInletVelocity;
             flowRate  0.2;
             value     uniform (0 0 0); }
```

5.5 Studied Configuration

The studied configuration is a jet flow that interacts with a transverse surrounding flow. In this work a simplified version of this problem configuration is used so that general fluid flow behaviour and compressible supersonic flow parameters could be addressed. The simulation domain consists of a rectangular box attached to a convergent nozzle, as shown in figure 11. The choice of the orifice size and all other domain's dimensions is made based on the experimental study on high speed crossflows by *Santiago and Duton* [46], with an orifice diameter of $4mm$. Although Kawai & Lele [29] and Higgins & Schmidt [20] performed similar studies on more compact configurations, the present domain is big enough to eliminate the effects of the boundary conditions. To test different boundary conditions, the overall stability of the schemes and check for problems in the simulation set-up, initially a two-dimensional version of the problem has been used and is given in (figure 10). Table 1 shows the dimensions of the domain given in m. Note that only a single element is used along the Y-direction on the *MeshDict*.

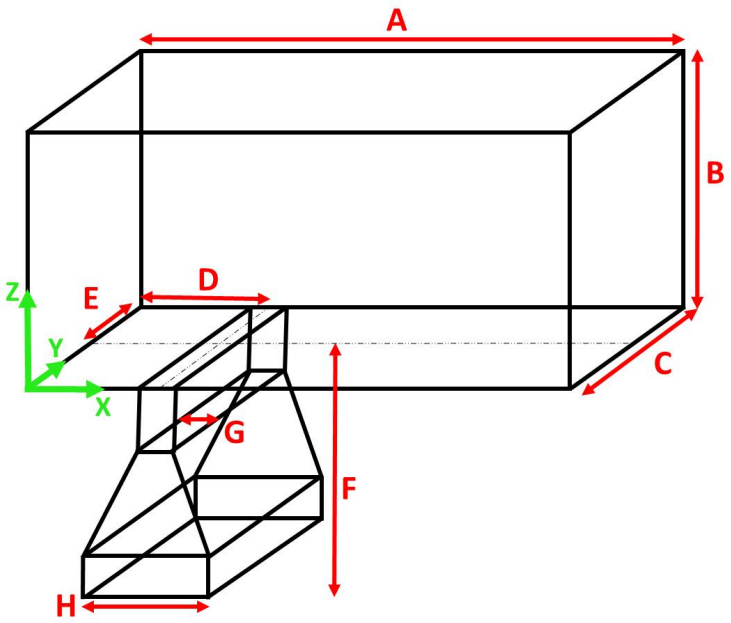

Figure 10: Physical 2D domain of the study.

The 3D mesh configuration is shown in figure 11. It is important to emphasize that the jet penetrates the main flow through a convergent nozzle to ensure sonic conditions at the orifice

exit (throat region). Ensuring sonic conditions at the is crucial so that the plenum is isolated from the jet development region. It is thus expected that disturbances at the jet/flow interaction will not propagate upstream. A mesh refinement zone was created around the orifice exit so that flow field details could be better resolved. The mesh generation, boundary conditions used as well as other parameters used to solve the problem will be discussed further on this report.

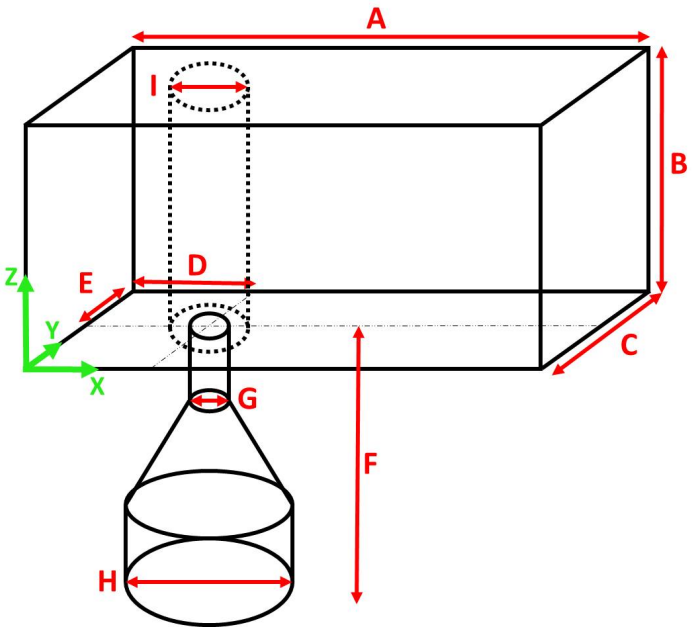

Figure 11: Physical 3D domain of the study.

Table 1: Prescribed domain dimensions

	Dimension
A (Length)	40 D
B (High)	20 D
C (Depth)	30 D
D (X-Distance from inlet)	10 D
E (Y-Distance from wall)	15 D
F (Nozzle length)	15 D
G (Orifice diameter)	1 D
H (Nozzle inlet diameter)	5 D
I (Mesh refinement region diameter)	3 D

5.6 Mesh Generation

The mesh was created using *blockMesh*, which is one of the simplest OpenFoam tools for grid generation. It is used to create structured hexahedral grids and based on the inputs from the user, *blockMesh* writes files used by OpenFoam to identify faces, cells and boundaries of the domain. The *MeshDict* file is located in the *constant* directory and it contains the following information about the mesh:

- **Vertices**

  In this section, the vertex coordinates of the hexahedral blocks that compose the simulation's domain are listed. The vertices are numbered in the ascending order, where the first vertex defined gets the label *0* and so on.

- **Edges**

  This is the part where the *arcs* (curvature of the edges) between 2 vertices are defined. This is needed because each edge connecting two vertices are assumed to be straight. In this project's case, this feature has been used to set the curvatures of the jet nozzle.

- **Blocks**

  In this section the blocks that form the simulation domain are defined: They are an exploded version of the domain into hexahedral blocks. The block is oriented following the convention that the normal points to the block exterior, thus, the bottom face vertices should be ordered in the counter clockwise direction followed by the correspondent vertices from the upper face. This section also defines i.e., the number of elements in each direction of the box may be chosen and the cell expansion ratios are set.

- **Patches**

  In this part of the mesh information provided to define the boundaries of the domain. Each boundary name (inlet, outlet, wall, obstacle, etc) has faces assigned to it and they can be defined as *patches* for common boundaries and *empty* for boundaries of 2D cases where 2 of the faces of the blocks do not take part in the calculations.

It is interesting to highlight that, before choosing *blockMesh*, another mesh generation program called *SALOME 2015.2* was used to create unstructured tetrahedral grid elements. *SALOME 2015.2* is a more intuitive and graphic-friendly software but due to conversion problems to *OpenFoam* format, as well as unknown errors when trying to use other element types, *SALOME* was discarded. The chosen software only allows hexahedral elements which is not a constraint to the present study, since hexahedral elements have been found to provide for adequate and efficient solutions.

2D

The first studied configuration is a two-dimensional one, given in figure 10, which has been divided into hexahedral blocks as shown in figure 12. This figure shows that the 2D configuration is composed of 3 blocks for the free-stream part and 3 others form the jet nozzle.

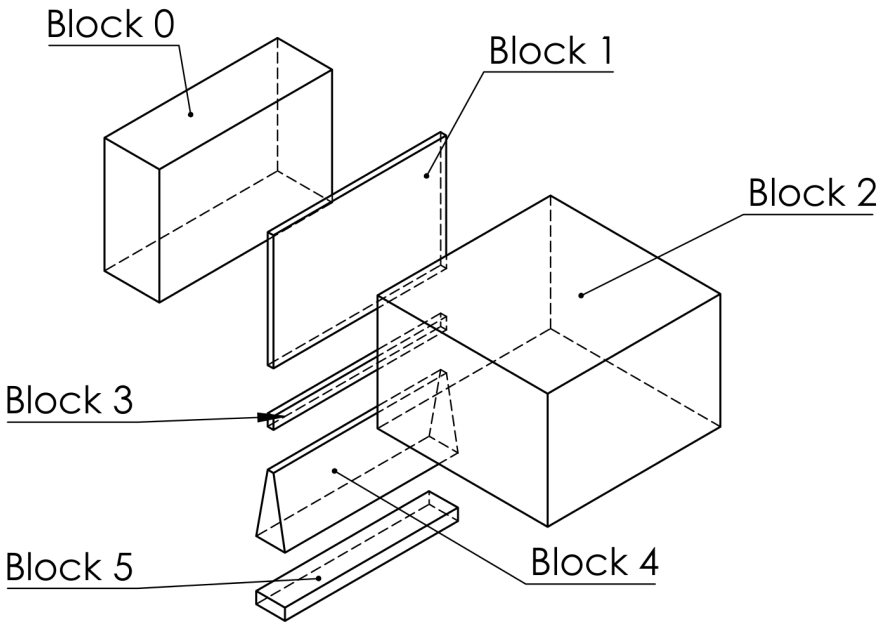

Figure 12: 2D domain's configuration divided into hexahedral blocks.

After identifying the blocks that compose the domain, the vertices have been labelled (28 vertices total) so the normal vectors of the faces point outwards the blocks, and are defined accordingly in the patch section of the *MeshDict* dictionary.

Figure 13 shows an example of the final result of the 2D mesh used to perform the

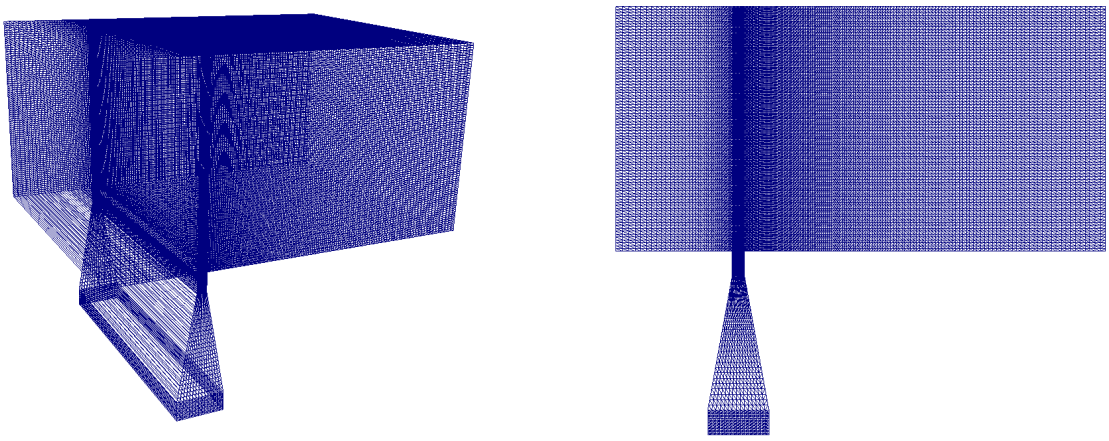

Figure 13: Wireframe views of the 2D mesh.

Table 2: Two-dimensional mesh information

Number of points	27032
Number of cells	13225
Maximum aspect ratio	12.5467
Maximum mesh skewness	0.223953
Maximum mesh non-orthogonality	10.8082
Elements growth ratio	0

numerical simulations of this work. For resolution and clarity reasons, the elements had their sizes changed so the figure could fairly represent how the mesh is. Table 2 gives important mesh information and also more details regarding the mesh dimensions and geometrical configuration are described in section 5.5, on page 26. It is interesting to emphasize that to keep the problem stable, the *Courant-Friedrichs-Lewis number* (equation 20) should be complied. To meet this criteria with a maximum velocity allowance of 1000 m/s in the X-direction and of 700 m/s in the Z-direction, the simulation's time step should not exceed 1.75e-6 seconds.

$$\frac{u_x \triangle t}{\triangle x} + \frac{u_z \triangle t}{\triangle z} \leqslant C_{max} = 1 \tag{20}$$

3D

A 3D mesh configuration, given in figure 11, has also been studied. Similar meshing generation processes of the 2D grid are used, with exception to the nozzle that is a cylindrical convergent

nozzle. This is a more complex mesh configuration, since there are non-orthogonal edges to be defined and, also, a very careful criteria for the blocks division (31 blocks in total). Figures 14 and 15 show the hexahedral blocks that form the 3D domain, with a mesh refinement region around the exit of the nozzle.

The grid has been designed to resolve the critical details of the flow field, such as the jet orifice exit region.

Similarly to the two-dimensional mesh, the blocks vertices have been labelled and defined as the boundaries of the domain (*crossflow inlet*,*crossflow outlet*,*nozzle inlet*,*walls* or *side patches*).

The mesh created for this work has been based on the publications listed in table 3. As it may be observed, the present mesh is very coarse when compared to the previous works, mainly because of the computational capability restriction: The simulations here were run in a Intel® Core™ i7 with 8 processors @ 2.50GHz with 378.8 GB disk space, whereas the works published used clusters with larger computational capability.

Table 3: Comparison between grids from the literature and the present mesh.

Owner	Domain's range			Number of elements
	L	H	D	
Chai and Mahesh, 2011	40D	20D	30D	25 million
Peterson and Candler, 2010	35D	16D	16D	13.6 million
Kawai and Lele, 2009	30D	13.3D	24D	10.5 million
Higgins and Schmidt, 2007	12D	8.25D	19.05D	2.9 million
Aline Wilm Pinto, 2016 (2D)	40D	20D	30D	13.2 thousand
Aline Wilm Pinto, 2016 (3D)	40D	20D	30D	1.26 million

Figure 16 shows the final three-dimensional mesh generated in this work. Table 4 lists important mesh information and more details regarding the mesh dimensions and geometrical configuration are described in section 5.5, on page 26. To get a Courant number below 1 (equation 20) and based on the velocities values of the 2D mesh (allowance of 1000 m/s in the X-direction and of 700 m/s in the Z-direction), the simulation's time step should not exceed 1.75e-6 seconds.

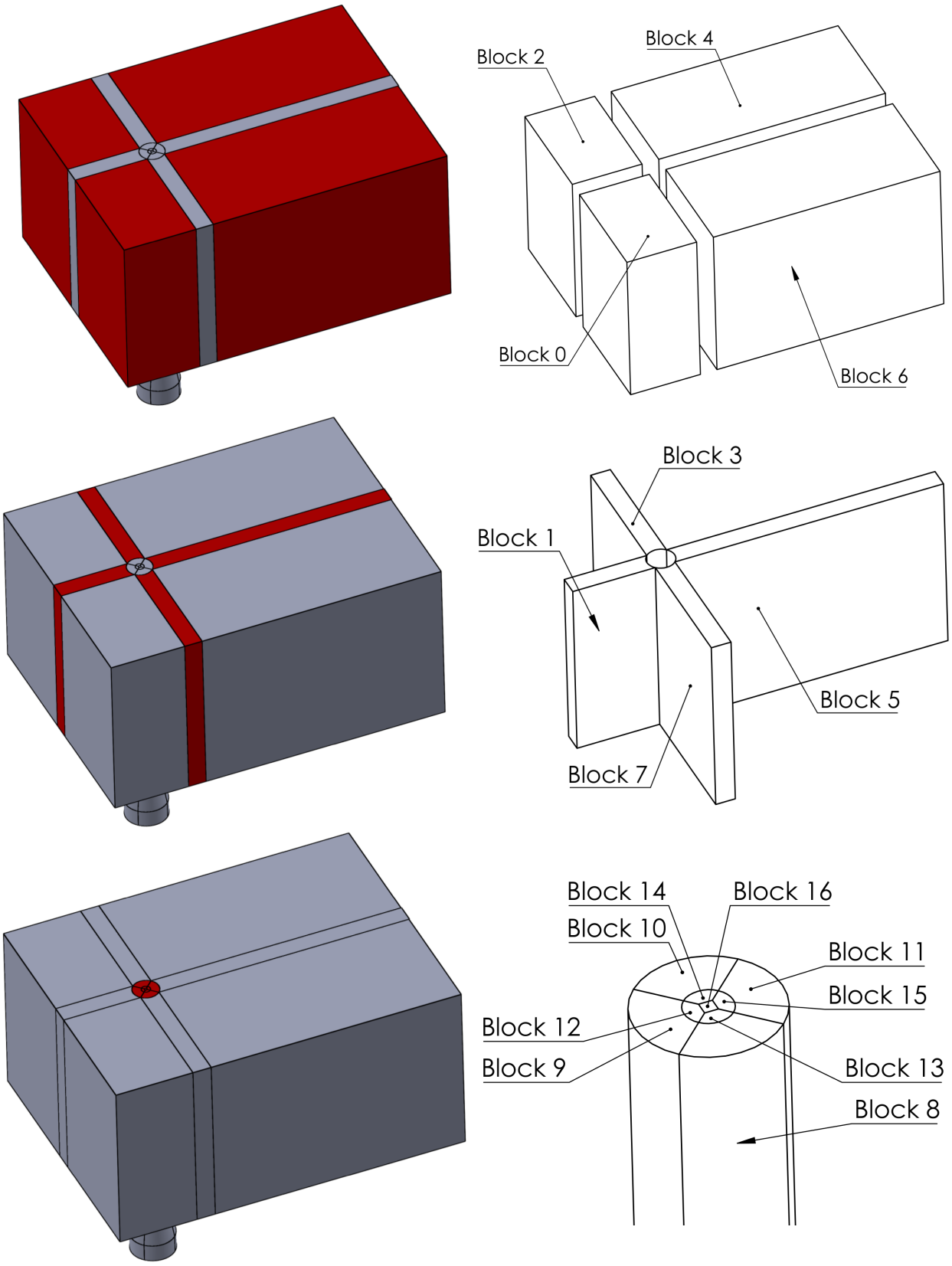

Figure 14: 3D domain's configuration of the free stream flow divided into hexahedral blocks.

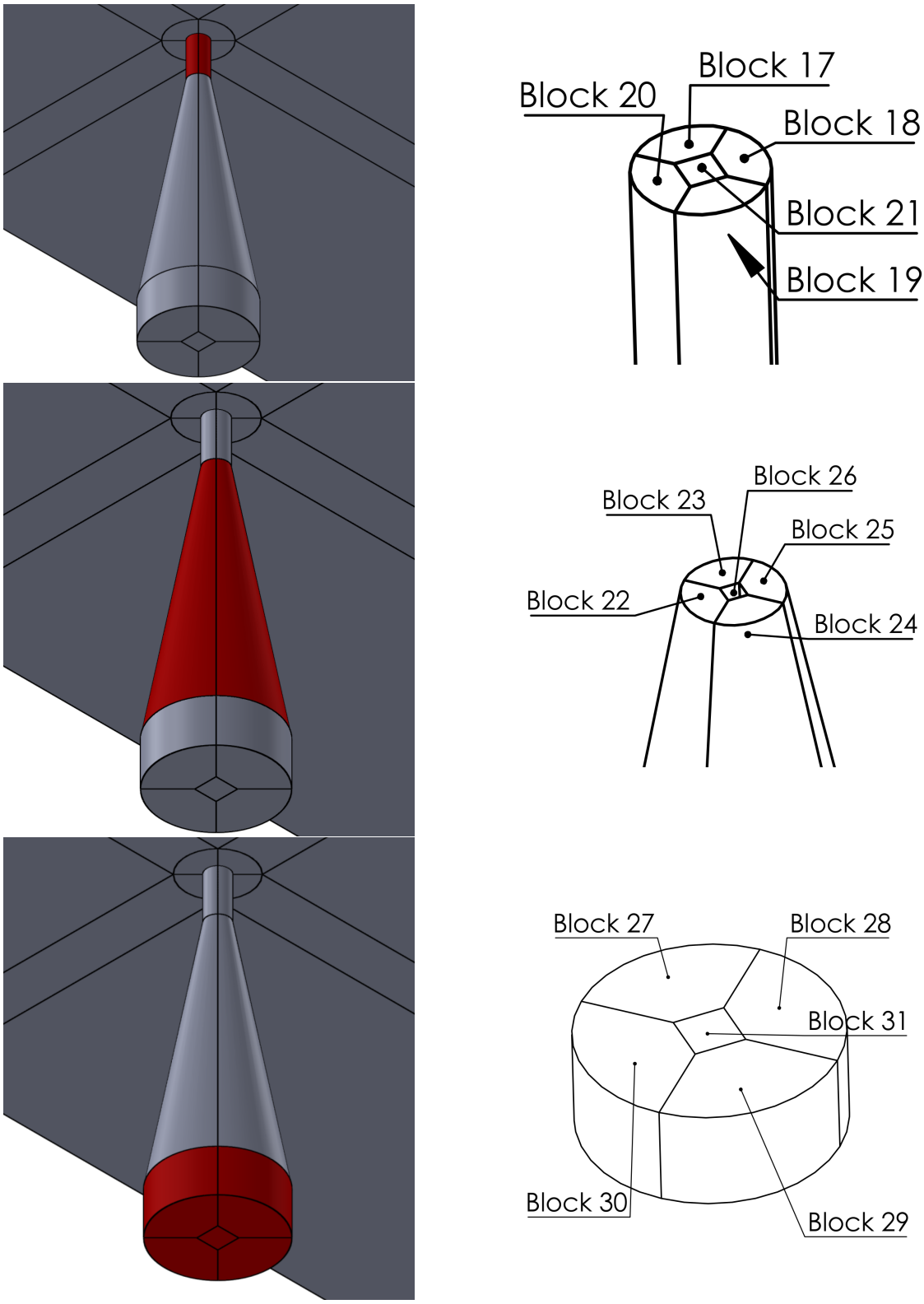

Figure 15: 3D domain's configuration of the jet nozzle divided into hexahedral blocks.

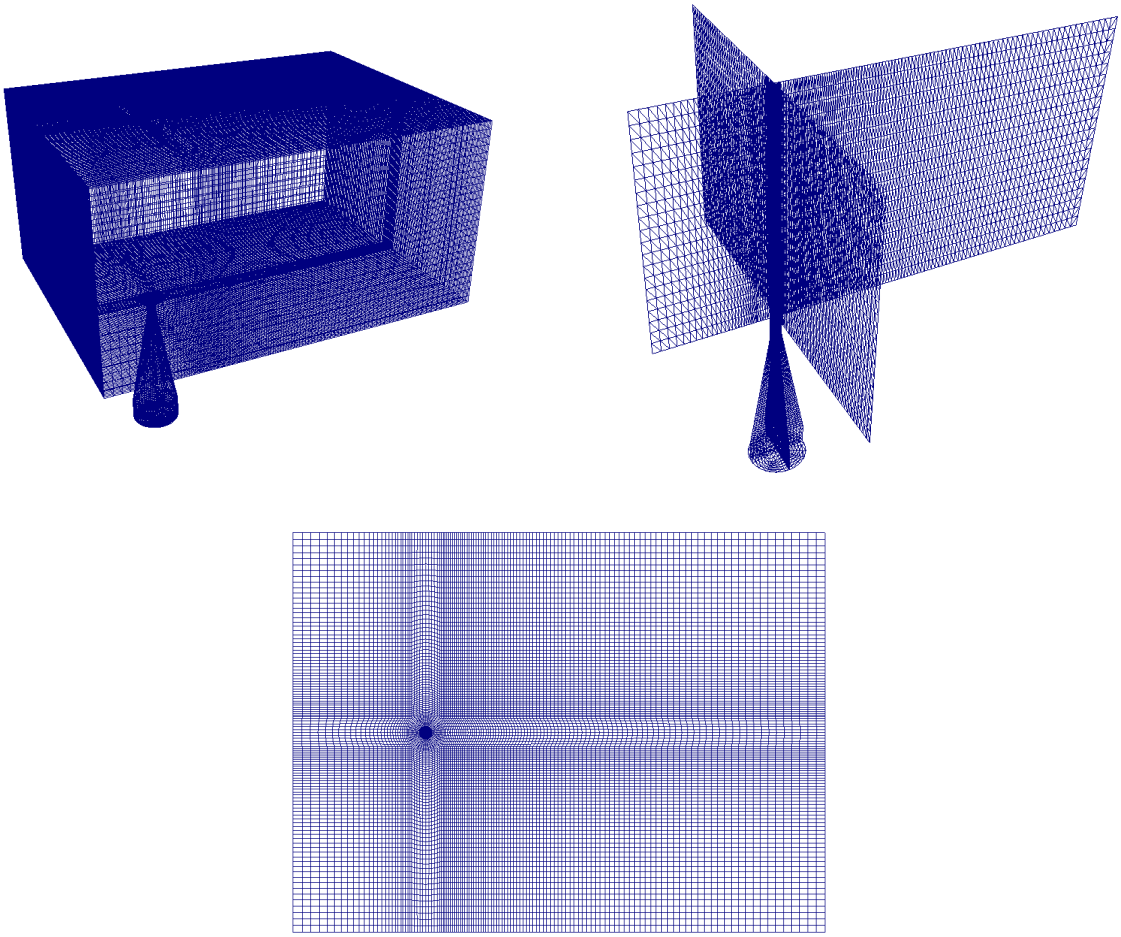

Figure 16: Wireframe views of the 3D mesh.

Table 4: Three-dimensional mesh information

Number of points	1302856
Number of cells	1266750
Maximum aspect ratio	16.9078
Maximum mesh skewness	1.28206
Maximum mesh non-orthogonality	40.3831

5.7 Problem Statement

The simulations run in this project considered a constant nozzle inlet velocity of 40 m/s and a constant mass flow rate at the free-stream inlet of 5 kg/s. Also, a fixed temperature of 300 K was set on both inlets. This leads to a pressure ratio between the jet and the freestream of 1.3 for the sonic nozzle case and 0.6 for the supersonic nozzle case.

6 Results and discussion

6.1 Preliminary Results

6.1.1 Parallel and Serial Simulations

Before running parallel simulations it is indispensable to perform a parallel/serial processing test, so as to determine the number of cells at each processor which decreases the computational time. This test has been performed and table 5 shows the CPU time required to run a simple case for different mesh sizes. The configuration adopted is that of a forward facing step under supersonic flow conditions, which is an *OpenFoam* tutorial case.

Table 5: Parallel and serial processing CPU times.

Total number of cells	***Total CPU time***	
	1 processor	***8 processors***
252	0.15 s	0.27 s
1008	0.46 s	0.54 s
4032	2.6 s	2.39 s
9072	9.49 s	5.32 s
16128	21.27 s	13.42 s
25200	44.26 s	33.11 s
36288	81.17 s	61.43 s
100800	434.66 s	369.78 s
226800	1563.54 s	1385.4 s

The mesh configuration adopted for this test is shown in figure 17. The only different between each run was the level of grid refinement, i.e., the total number of cells. The case set-up used the same solver as the one employed to perform all the other simulations of this project. The simulation physical end time was fixed at 0.5 s, with a maximum Courant number of 0.2. Adaptive time step is used to ensure that. The computer used for this study uses *Linux Ubuntu 14.04*, processor *Intel® Core™ i7-4710HQ*, with 8 GB of memory.

Figure 18 shows the performance of both serial and parallel simulations. This figure shows that for grids with more than 4032 cells, parallel processing always leads to an improvement of CPU time. Indeed, for an average number of 504 cells per processor, a parallel simulation with 8 processors is 8% faster than a serial one. Even if this is a modest improvement only, all simulations

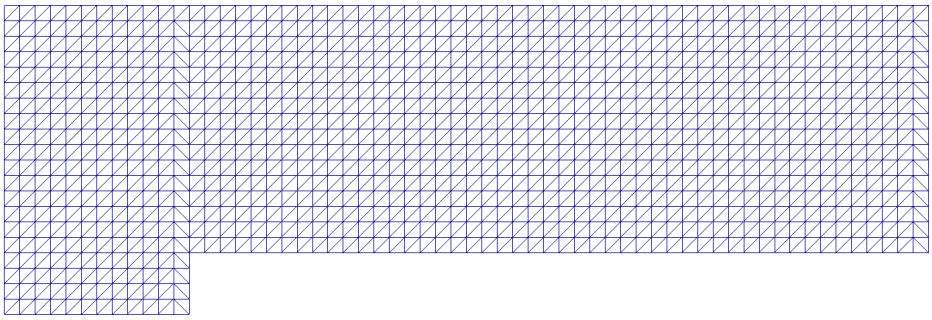

Figure 17: Parallel/serial computational domain.

have been performed in parallel here. A more rigorous speed up test has not been performed and is out of the scope of this study.

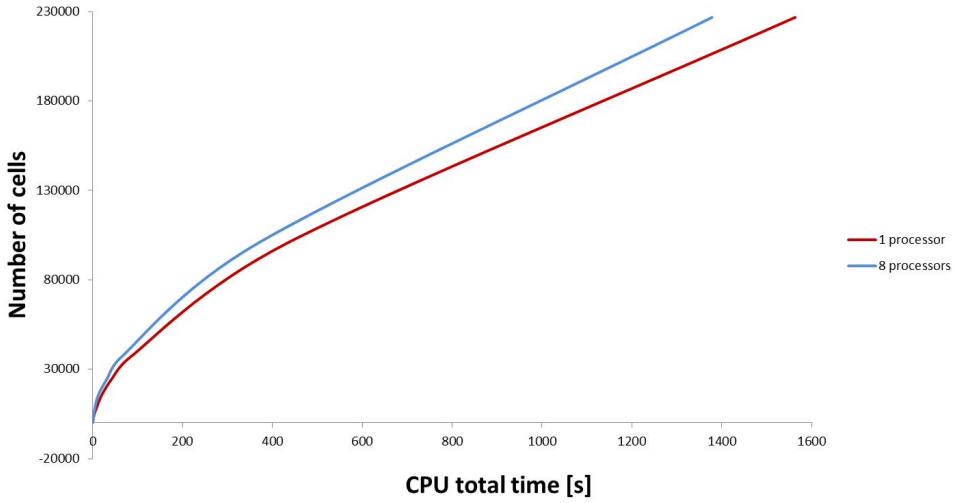

Figure 18: Parallel processing computational time results.

6.1.2 Solver and Boundary Layer

In order to understand the baheviour of the solver used in this project (*rhoCentralDyMFoam*) and to test the boundary conditions at the walls, tests with both 2D and 3D meshes were performed for a simple channel with a uniform inlet velocity.

The boundary conditions for pressure and temperature were set as *zeroGradient* for all domain patches, whereas a velocity boundary condition with *fixedValue* of 0 m/s on the walls and

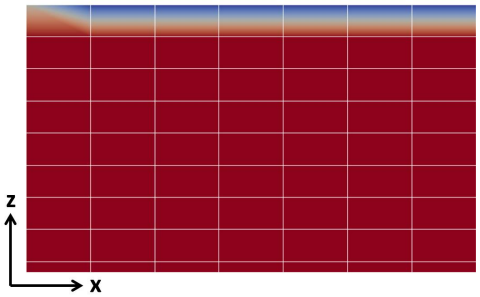

Figure 19: Zoom view of the simple channel domain and grid resolution for a preliminary test.

555 m/s on the X-direction on the inlet were imposed. In the X-direction the mesh was divided in hexahedral elements with 1.6 mm width and 1.4 mm height. The inlet velocity is equivalent to a Mach number of 1.59. A *zeroGradient* condition for velocity was also set at the channel outlet. The simulation was run for 0.05 s.

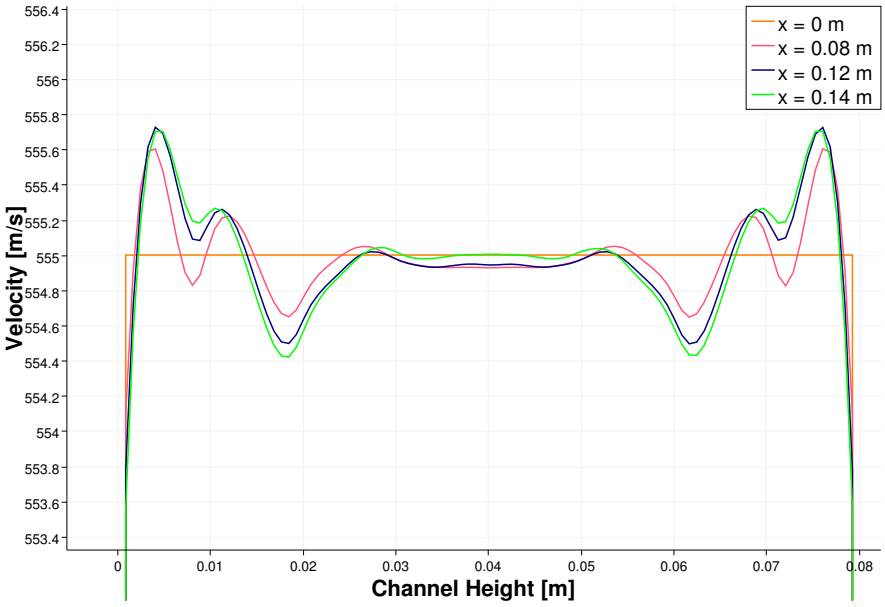

Figure 20: Velocity profile for 4 different sections for a no-slip boundary condition wall.

Figure 19 shows the near-wall region of the mesh used, a rectangular box with *0.16 x 0.12 x 0.14 m*. This figure clearly shows that the used mesh is not sufficient to capture the boundary layer. The velocity profiles for 4 different sections in the X-axis were analysed also, and are given in figure 20. It is possible to examine, in this figure, how the velocity profile develops along the X-direction and why a high grid resolution near the walls is desirable to avoid steep gradients and

resolve small scale variations. Since such a high resolution cannot be achieved within the study available time frame, resolving the boundary layers with an adequate mesh refinement has not been attempted.

6.1.3 Nozzle Fluid Flow

In order to study the fluid flow in the jet nozzle, simulations were run with this project's mesh with fluid flow only entering through the nozzle, i.e., with no cross flow. The desired behaviour is to have an increasing velocity accompanied by a pressure drop along the nozzle. The main reason of doing such study is to ensure that sonic conditions are found in the orifice exit given some specific nozzle-inlet conditions and, also, to verify if different wall boundary conditions affect the jet plume structure.

Two velocity boundary conditions for the walls were tested: *slip* and *fixedValue* of 0 m/s. All the tests had similar boundary conditions, i.e.: The velocity setting for the main flow inlet and outlet were *zeroGradient*, the temperature boundary condition was set as *zeroGradient* for all the domain patches, in exception to the nozzle inlet and the pressure was also set as *zeroGradient* in all the boundaries, letting it be adjustable to the other flow field parameters such as velocity and temperature.

The following items describe some of the preliminary tests performed and, also, their results. More information about the mesh can be found in section 5.6.

- **No-Slip Wall Boundary Condition for a Sonic Jet**

  The first test performed was for the fluid flow domain given in figure 10 . Fluid flow was set to enter the domain only through the nozzle inlet and all the other boundaries were set as outflow, with exception of the walls, i.e., the upper and bottom walls from the free stream region and also the nozzle walls. This test was configured so a sonic regime could be observed at the nozzle exit orifice, whereas the surrounding flow was at rest. The boundary conditions prescribed for this test are listed in table 6.

Table 6: Boundary condition list for the *no-slip* wall boundary condition and sonic jet preliminary test.

	Pressure [Pa]	**Temperature [K]**	**Velocity [m/s]**
Main Flow Inlet	*zeroGradient*	*zeroGradient*	*zeroGradient*
Nozzle Inlet	*zeroGradient*	*fixedValue, 300 K*	*flowRateInletVelocity, 1 kg/s*
Main Flow Walls	*zeroGradient*	*zeroGradient*	*fixedValue, (0 0 0) m/s*
Nozzle Walls	*zeroGradient*	*zeroGradient*	*fixedValue, (0 0 0) m/s*
Outlet	*zeroGradient*	*zeroGradient*	*zeroGradient*
Internal Field	*uniform 101325 K*	*uniform 300 K*	uniform (0 0 0) m/s

After some time, the flow fields given in figure 21 have been obtained. Note that the nozzle has a under-expanded behaviour: the pressure at the exit is higher than the free-stream environment. Also, it may be observed that compression and expansion waves form around the jet boundaries, which are separated by Mach disks. This phenomena is also observed in rocket engine nozzles and high-velocity aircrafts.

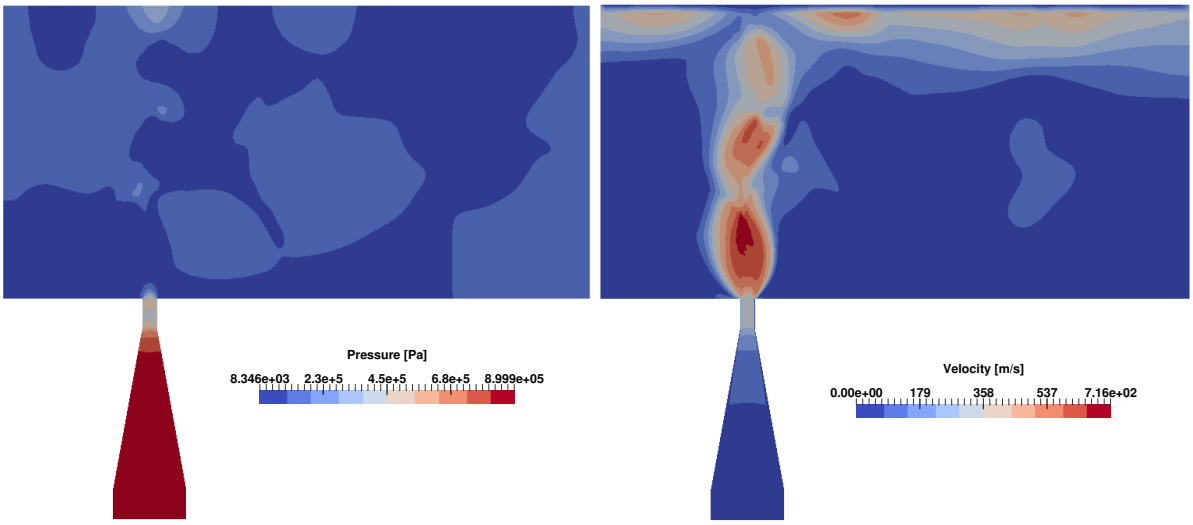

Figure 21: Pressure and velocity fields for the *no-slip* wall boundary condition and sonic jet preliminary test.

Velocity, Mach number, pressure and temperature evolution across the center of the nozzle are plotted in figure 21. In this figure it may be verified that the desired sonic conditions are actually obtained at the exit orifice.

Furthermore as shown in figure 22, both temperature and pressure decrease as the fluid flows inside the convergent nozzle as it could have been expected.

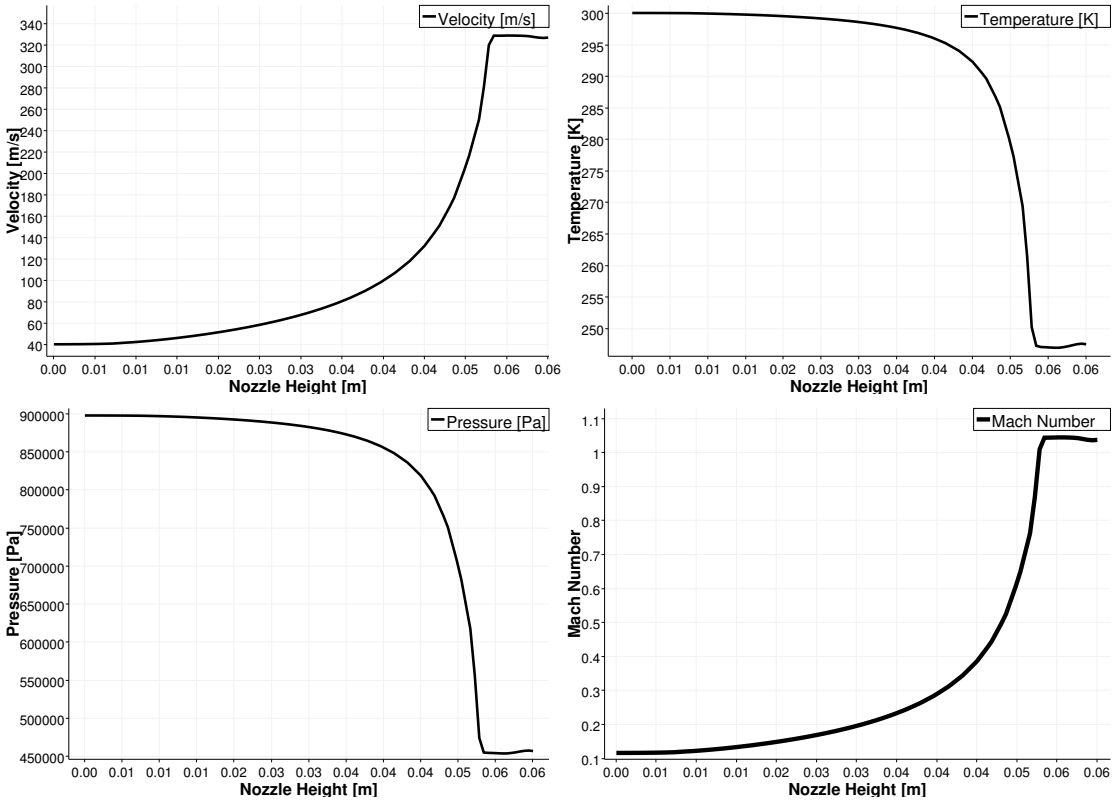

Figure 22: Nozzle behaviour for the *zeroGradient* wall boundary condition and sonic jet preliminary test

- **Slip Wall Boundary Condition for a Sonic Jet**

  The second jet test performed was similar to the one described above with exception to the walls that were set with a *slip* boundary condition.

  After the same number of iterations from the results of the *no-slip* wall boundary condition test, the flow fields observed in figure 23 were obtained. Again, the nozzle presents a under-expanded behaviour, meaning that the fluid discharges at an exit pressure greater that the external pressure, due to its incomplete expansion.

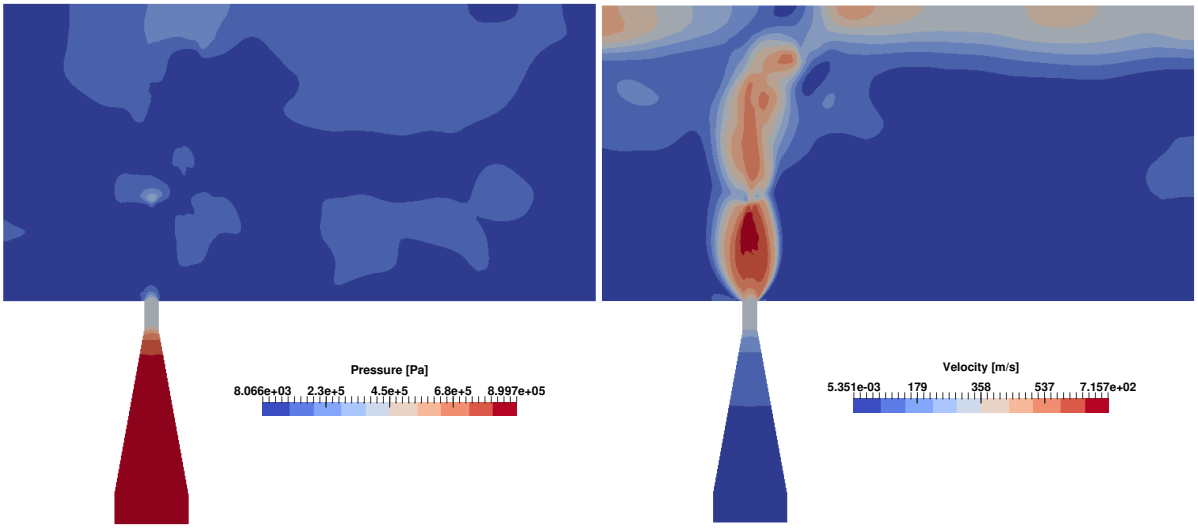

Figure 23: Pressure and velocity fields for the *slip* wall boundary condition and sonic jet preliminary test

Lines for the velocity, Mach number, pressure and temperature across the center of the nozzle were also plotted to confirm the flow behaviour with a *slip* condition on the walls. Differently from the *no-slip* boundary condition, *slip* walls, i.e.,normal velocities are zero while the tangential components are not, are well suitable in cases where viscous effects are negligible and the mesh resolution is not fine enough to capture the boundary layer thickness. Even though this is not a realistic description of the near-wall velocity behaviour, this condition is commonly used for coarse grids and symmetrical geometries.

Figure 24 shows the results obtained in terms of velocity, temperature, pressure and Mach number along the nozzle. As expected, very similar conditions compared to the *no-slip* case were found. Slight increase in the pressure at the neighbourhood of the jet orifice was observed for the *no-slip* wall boundary condition whereas in the *slip* wall case no changes were observed. However, this subtle difference did not show significant influence in the overall fluid flow structure.

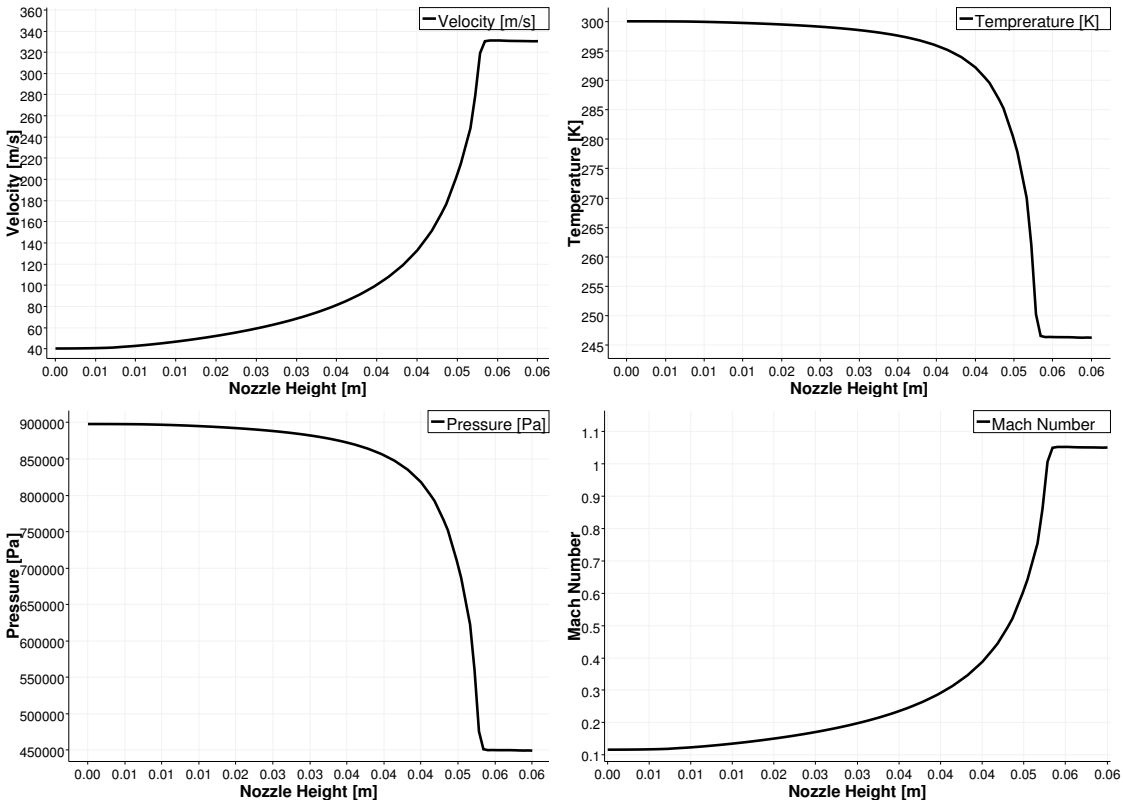

Figure 24: Nozzle behaviour for the *slip* wall boundary condition and sonic jet preliminary test.

From these two tests perfomed, it may be concluded that either *no-slip* or *slip* walls could be used to run the simulations with no significant changes to the flow behaviour.

- **Supersonic Jet**

  In order to assess the behaviour of a supersonic jet, a convergent-divergent nozzle configuration was used. This type of nozzle is designed to accelerate the subsonic flow in the convergent region until it reaches sonic conditions at the throat. Downstream the throat, the divergent section of the nozzle results in the a supersonic flow regime. The boundary conditions chosen are the same as those given in table 6 (no-slip conditions on the walls). Figure 25 shows the flow field behaviour, in terms of the pressure and velocity fields.

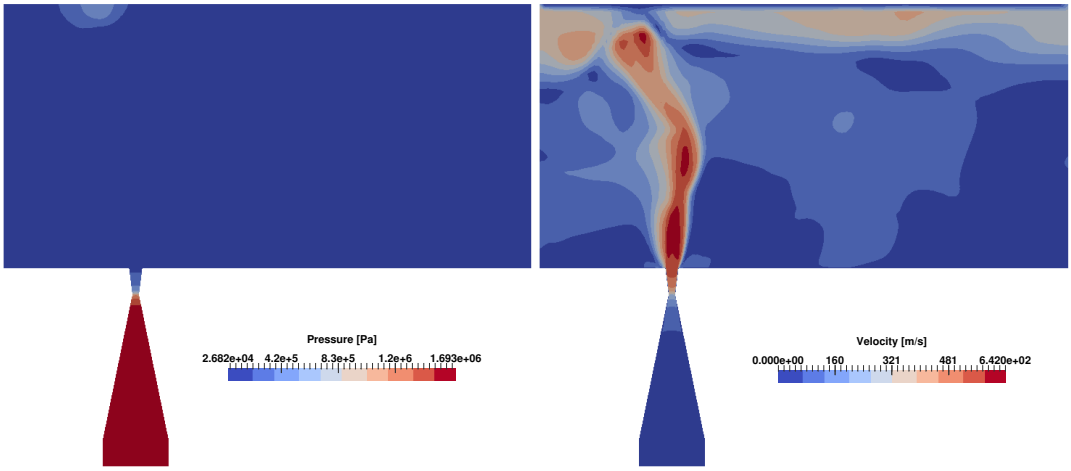

Figure 25: Pressure and velocity fields for the convergent-divergent nozzle with supersonic conditions at the jet orifice.

As it may be seen in figure 25, the convergent-divergent nozzle leads to a fully supersonic flow at its exit orifice.

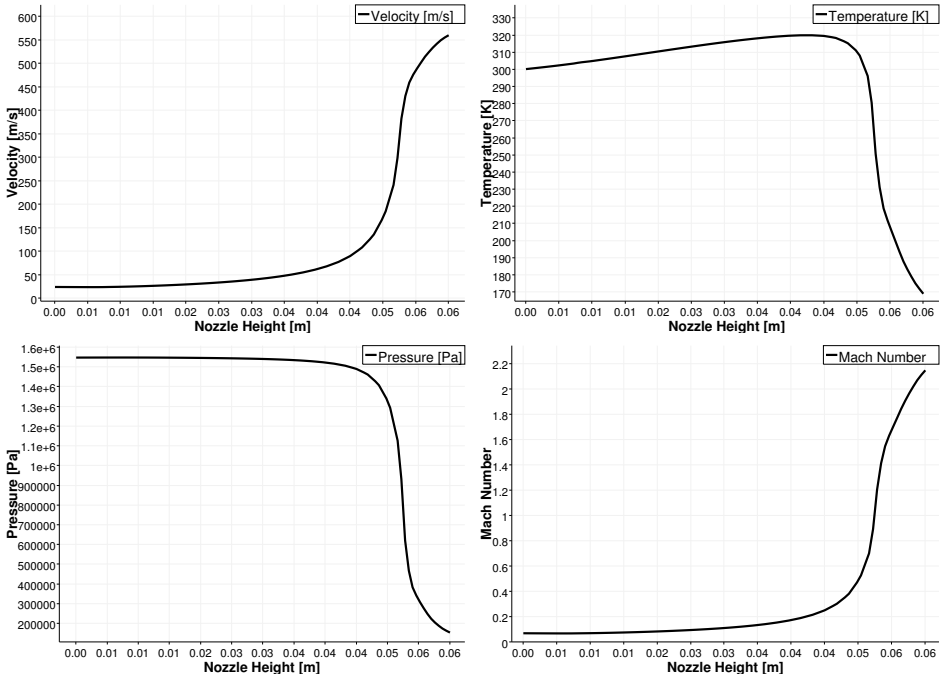

Figure 26: Nozzle behaviour for a supersonic jet.

More details of the flow across the nozzle are shown in figure 26, which depicts the velocity, temperature, pressure and Mach number evolution along the nozzle. This figure clearly shows that supersonic flow results at the nozzle exit section.

6.2 Sonic jet in subsonic crossflow

The boundary conditions set for this study are listed in table 7. The corresponding flow field results obtained for a sonic jet issuing into a subsonic cross flow are found in figure 27.

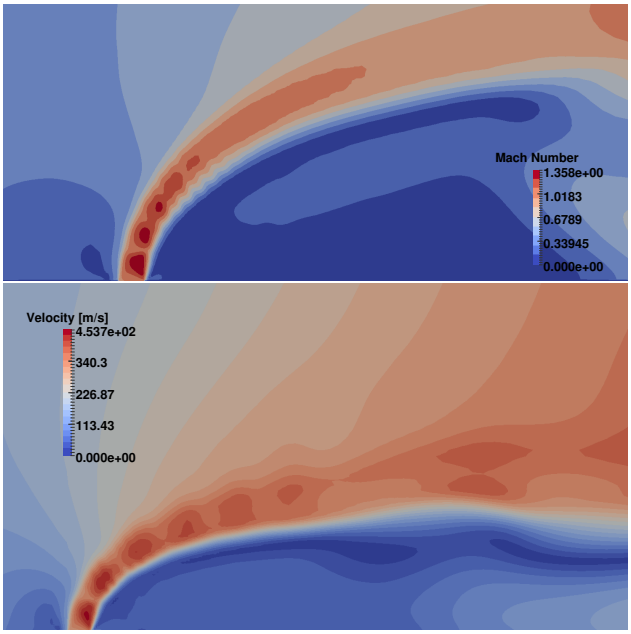

Figure 27: Mach number and velocity contours for a sonic jet issuing into a subsonic crossflow.

From the analysis of the flow field given in figure 27, Mach disk formation may be seen, as well as the influence of the cross flow on the bending direction of the jet plume. Because of the rather coarse grid resolution, vortex structures and boundary layer effects on the flow cannot be observed.

Figure 28 illustrates the comparison made between the velocity profiles from distances of 2,3,4 and 5 diameters from the main flow inlet. This figure is given for illustration purposes only, since the present case is a 2D flow field, whereas the compared literature data corresponds to a 3D configuration. The literature case that was used to make the comparison had a jet Mach number of 3.73, density ratio between the jet and main flow inlet of $\rho_j/\rho_\infty = 47.1$ and pressure ratio of $p_j/p_\infty = 49.1$.

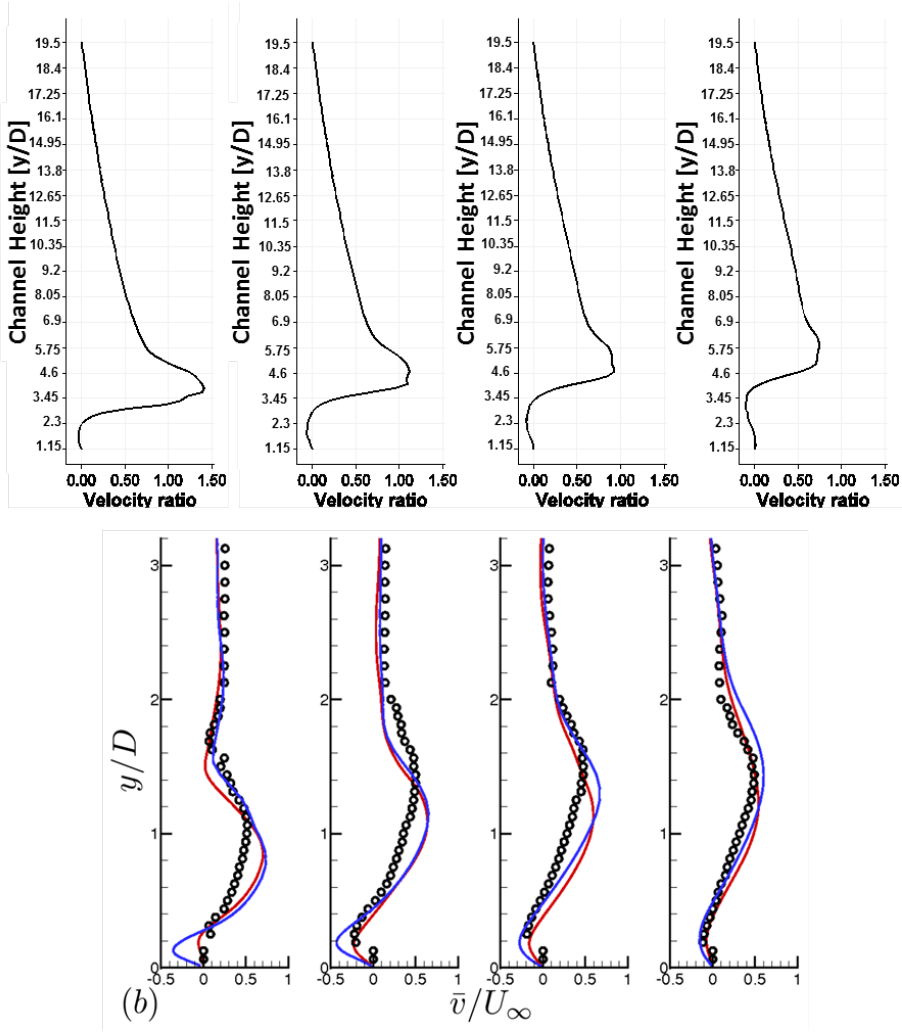

Figure 28: Comparison between literature data, *Chai and Mahesh, 2011*, and present work results for X-distances of 2, 3, 4 and 5 diameters from the main flow inlet, respectively.

Table 7: Boundary conditions used to perform the simulation of a sonic jet issuing into a subsonic crossflow.

	Pressure [Pa]	**Temperature [K]**	**Velocity [m/s]**
Main Flow Inlet	*zeroGradient*	*fixedValue, 300 K*	*flowRateInletVelocity, 5 kg/s*
Nozzle Inlet	*zeroGradient*	*fixedValue, 300 K*	*fixedValue, (0 0 40) m/s*
Main Flow Walls	*zeroGradient*	*zeroGradient*	*fixedValue, (0 0 0) m/s*
Nozzle Walls	*zeroGradient*	*zeroGradient*	*fixedValue, (0 0 0) m/s*
Outlet	*zeroGradient*	*zeroGradient*	*zeroGradient*
Internal Field	*uniform 101325 K*	*uniform 300 K*	uniform (0 0 0) m/s

It is interesting to note that both experimental and numerical literature data had a velocity ratio between the main flow inlet and the jet exit orifice of 4, which is nearly double of the one

adopted on the simulations of this project. Nevertheless, the jet penetration in the present 2D case is much higher than in the 3D experiments/calculations. This is not surprising, given the fact that a round jet leads to a much smaller flow blockage than the planar (2D) jet.

6.3 Supersonic jet in subsonic crossflow

The boundary conditions set for this simulation were similar to the sonic jet configuration, and in this case the convergent-divergent nozzle is responsible for assuring supersonic regime at the exit orifice.

The results obtained for a supersonic jet issuing into a subsonic crossflow may be observed in figure 29, where the Mach number contours are shown, together with stream lines.

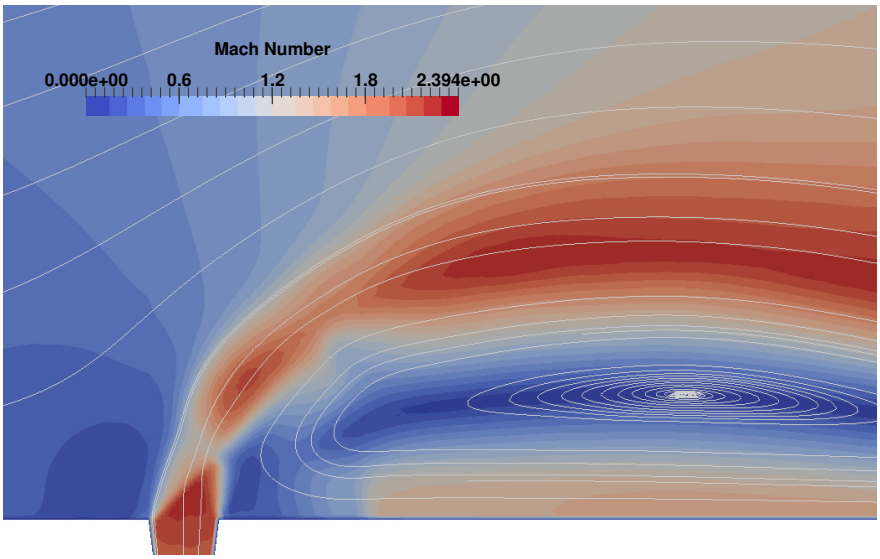

Figure 29: Mach number and velocity contours for a supersonic jet issuing into a subsonic crossflow.

These results could be qualitatively compared to the flow structure obtained by *Chai and Mahesh, 2011*, given in figure 30. Observing both figures, some similarities can be found, such as the Mach disk formation as well as the jet boundaries caused by the reflection of expansion waves. From the instantaneous flow field in figure 30, it is also possible to evidence a recirculation region upstream of the jet. In the same region, the flow field is possibly subsonic, thus no shocks are formed.

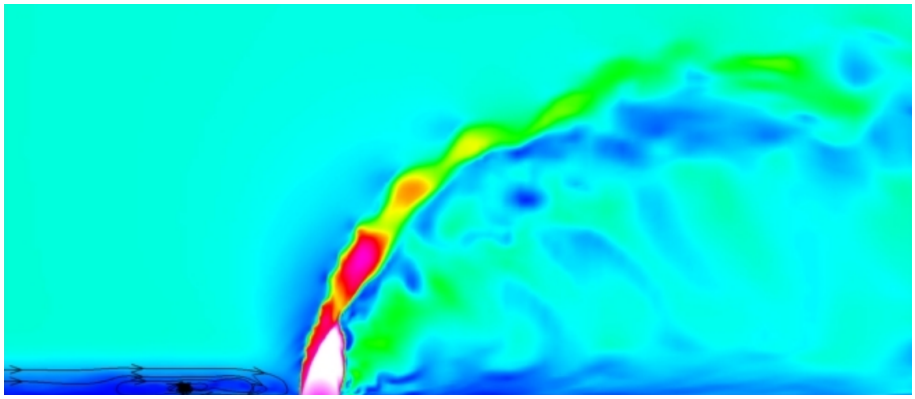

Figure 30: Flow structure found by *Chai and Mahesh, 2011* for a supersonic jet issuing into a subsonic crossflow.

7 Conclusion

In this study, numerical simulations were performed with an intention to study both sonic and supersonic exit orifice nozzle regimes. Preliminary tests were performed to assure proper case configuration, thus leading to representative final results. It was found that the simulation of a sonic jet issuing in to a subsonic cross flow presented results comparable to a numerical study from *Chai and Mahesh, 2011*. For the simulation of a supersonic jet into a subsonic cross flow, a similar flow structure was found between literature records, *Chai and Mahesh, 2011*. The Mach disk formation and the jet boundaries caused by the reflection of expansion waves when the jet meets the surrounding cross flow were observed.

Unfortunately due to the lack of time available for resolving all the problems found during the project development, three-dimensional simulations were not successfully performed. However, the exposure to such numerical resources has improved my knowledge on those tools, allowing to build a problem case from zero and to collect results.

It is also important to highlight that this project was made over no pre-setted case, so all the grids, methods, case set-up, tests, etc had to be built from zero stack. Furthermore, since all the resources used in this project were brand new to me, one of the most important target of this work was to get familiarized with the tools used in numerical studies.

Future development of this work would be to perform the three-dimensional simulations, as well as to test supersonic free-stream crossflow inlet boundary condition.

References

[1] Ajersch, P., Zhou, J.M., Ketler, S. , Salcudean, M. and Gartshore, I.S. *Multiple jets in a cross-flow: Detailed measurements and numerical simulations* International Gas Turbine and Aero-engine Congress and Exposition, 1995.

[2] Ben-Yakar, A. *Experimental investigation of mixing and ignition of transverse jets in supersonic crossflows* Doctor of Philosophy Dissertation - Stanford University, 2000.

[3] Ben-Yakar, A., Mungal, M.G. and Hanson, R.K. *Time evolution and mixing characteristics of hydrogen and ethylene transverse jets in supersonic crossflows* Physics of Fluids - 18, 026101, 2006.

[4] Beresh, S.J., Henfling, J.F., Erven, R.J. and Spillers, R.W. *Penetration of a transverse supersonic jet into a subsonic compressible crossflow* AIAA Journal vol.43, No.2, 2005.

[5] Ccacya,A.O.R. and Figueira da Silva, L.F.F. *Characterization of multi-jet turbulent flames in crossflow using Stereo-PIV and OH-PLIF* Fire Safety Journal, 2015.

[6] Chai, X. and Mahesh, K. *Simulations of high speed turbulent jets in crossflows*. 49th AIAA Aerospace Sciences Meeting, 2011.

[7] Chai X., Iyer P.S. and Mahesh K. *Numerical study of high speed jets in crossflow* Journal of Fluid Mechanics vol. 785 (152-188), 2015.

[8] Clemens, N.T. and Mungal, M.G. *Large-scale structure and entrainment in the supersonic mixing layer* Journal of Fluid Mechanics vol.284, 1995. pp. 171-216

[9] Davidson, P.A. *Turbulence - An introduction for scientists and engineers* Oxford - Second edition, 2015.

[10] Demuren, A.O. *Characteristics of three-dimensional turbulent jets in crossflow* International Journal of Engineering Science Vol.31 No.6, 1993, pp. 899-913

[11] Doom,J. , Hou, Y. and Mahesh, K. *A Numerical method for DNS/LES of turbulent reacting flows* Journal of Computational Physics, 226. pp. 1136–1151

[12] Feistauer, M., Felcman, J. and Straskraba, I. *Mathematical and computational methods for compressible flow* Oxford Science Publications, 2003.

[13] Felcman M.F.J. and Straskraba I. *Mathematical and computational methods for compressible flow* Oxford Science Publications - First Edition, 2003.

[14] Ferziger, J.H. and Peric, M. *Computational methods for fluid dynamics* Springer, 2002.

[15] Griebel, M., Dornseifer, T. and Neunhoeffer, T. *Numerical simulation in fluid dynamics - A practical introduction* Siam, 1998.

[16] Gruber, M.R., Nejadt, A.S. and Chen, T.H. *Mixing and penetration studies of sonic jets in a Mach 2 freestream* Journal of Propulsion Power vol.11 No.2 (315-323), 1997.

[17] Han, D. and Mungal, M.G. *Direct measurement of entrainment in reacting/nonreacting jets* Stanford University. The Combustion Institute, Elsevier Science In.c, 2001.

[18] Hasselbrink, E.F. Jr and Mungal, M.G. *Transverse jets and jet flames. Part 1. Scaling laws for strong transverse jets* Journal Fluid Mechanics Vol.443, 2001. pp. 1-25

[19] Hasselbrink, E.F. Jr and Mungal, M.G. *Transverse jets and jet flames. Part 2. Velocity and OH field imaging* Journal Fluid Mechanics Vol.443, 2001. pp. 27-68.

[20] Higgings K. and Schmidt S. *Simulation of a sonic jet injected into a supersonic cross-flow* 16th Australasian Fluid Mechanics Conference (608-612), 2007.

[21] Hoffmann K.A. and Chiang S.T. *Computational fluid dynamics* Engineering Education System, Forth Edition - Volume 1, 2004.

[22] Holdeman, J.D. *Mixing of multiple jets with a confined subsonic crossflow* Program of Energy Combustion Science Vol.19, 1993, pp. 31-70.

[23] Ibrahim, I.M., Gutmark, E.J. *Dynamics of single and twin circular jets in cross flow* Proceedings of the 44th AIAA Aerospace Sciences Meeting and Exhibit, 2006.

[24] Isaac, K.M., Jakubowski, A.K. *Experimental study of the interaction of multiple jets with a cross flow* AIAA Journal vol.23 No 11, 1985. pp. 1679–1683.

[25] Johari, H. ,Pacheco-Tougas, M. and Hermanson, J.C. *Penetration and mixing of fully modulated* Turbulent Jets in Crossflow AIAA Journal vol.37 No.7, 1999.

[26] Johnson, R.W. *The handbook of fluid dynamics* CRC Press, 1998.

[27] Kamotani, Y. and Greber, I. *Experiments on a turbulent jet in a cross flow* AIAA Journal vol.10, No.11, 1972

[28] Kawai S. and Lele S.K. *Large-eddy simulation of jet mixing in a supersonic turbulent crossflow* Center for Turbulence Research Annual Research Briefs, 2008.

[29] Kawai S. and Lele S.K. *Dynamics and mixing of a sonic jet in a supersonic turbulent crossflow*. Center for Turbulence - Annual Research Briefs (285-298), 2009.

[30] Ki, S.W. and Benson, T.J. *Fluid flow of a row of jets in crossflow—A numerical study*. AIAA Journal vol.31, No.5 , 1993.

[31] Kolar, V., Takao, H., Todoroki, T., Savory, E., Okamoto, S., Toy, N. *Vorticity transport within twin jets in cross flow*. Experimental Thermal Fluid Science 27, 2003. pp. 563–571.

[32] Kundu P. K., Cohen I. M. and Dowling D. R. *Fluid mechanics* Elsevier - Fifth Edition, 2012.

[33] Kurganov A. and Tadmor E. *New high-resolution semi-discrete central schemes for Hamilton–Jacobi equations* Journal of Computational Physics 160 (720–742), 2000.

[34] Lesieur, M. *Turbulence in fluids* Kluwer Academic Publishers, 1997.

[35] Magnus Winter *Benchmark and validation of OpenSource CFD codes, with focus on compressible and rotating capabilities, for integration on the SimScale platform* Master's thesis

in Engineering Mathematics & Computational Sciences. Department of Applied Mechanics. Chalmers University of Technology, 2013.

[36] Mahesh K. *The interaction of jets with crossflow* Annual review Fluid Mech (379-407), 2013.

[37] McDaniel, J.C. and Graves, J. *A laser-induced-fluorescence visualization study of transverse, sonic fuel injection in a nonreacting supersonic combustor* Journal of Propulsion vol.4, No.6, 1988. pp. 591-597.

[38] Menon, R. and Gollahalli, S.R. *Combustion characteristics of interacting multiple jets in cross flow* Combustion Science and Technology Vol.60, 1988 pp. 375-389

[39] Muppidi, S. and Mahesh, K. *Direct numerical simulation of round turbulent jets in crossflow* Journal of Fluid Mechanics vol.574, 2007. pp. 59-84.

[40] Muppidi, S. and Mahesh, K. *Study of trajectories of jets in crossflow using direct numerical simulations* Journal of Fluid Mechanics vol.530, 2007. pp. 81-100.

[41] Naik-Nimbalkar, V.S., Suryawanshi, A.D., Patwardhan, A.W., Banerjee, I., Padmakumar G. and Vaidyanathan G. *Twin jets in cross-flow* Chemical Engineering Science, 2011.

[42] Papamoschou, D. and Hubbard, D.G. *Visual observations of supersonic transverse jets* Experimental Fluids - 14 (468-476), 1993.

[43] Peterson, D.M. and Candler, G.V. *Supersonic combustor fuel injection simulations using a hybrid RANS/LES approach* AIAA Journal vol.43, No.2, 2005. 48th AIAA Aerospace Sciences Meeting, New Horizons Forum and Aerospace Exposition. AIAA 411, 2010.

[44] Pope, S.B. *Turbulent flows* Cambridge University Press, 2000.

[45] Rothstein, A.D. and Wantuck, P.J. *A study of the normal injection of hydrogen into a heated supersonic flow using Planar Laser-Induced Fluorescence* AIAA Paper 92-3423, 1992.

[46] Santiago, J.G. and Duton, C.J. *Velocity measurements of a jet injected into a supersonic crossflow* Journal of Propulsion and Power vol.13 No.2, 1997. pp. 264 - 273.

[47] Sau, R. and Mahesh, K. *Dynamics and mixing of vortex rings in crossflow* Journal of Fluid Mechanics Vol.604, 2008. pp. 389-409.

[48] Schetz, J.A. and Billlig, F.S. *Penetration of gaseous jets injected into a supersonic stream* Journal of Spacecraft Rockets, vol.3 - No.11, 1966.

[49] Shapiro A.H. *The dynamics and thermodynamics of compressible fluid flow* John Wiley & Sons - Volume 1, 1953.

[50] Sherif, S.A. and Pletcher, R.H. *Measurements of the flow and turbulence characteristics of round jets in crossflows* Journal of Fluids Engineering Vol.111, 1989.

[51] Wuthrich B. *Simulation and validation of compressible flow in nozzle geometries and validation of OpenFOAM for this application* Computational Science and Engineering Master Thesis, 2007.

[52] Young S.N. *A review on empirical correlations for jet/spray trajectory of liquid jet in uniform cross flow* International journal of spray and combustion dynamics Vol.7 No4 (283-314), 2013.

[53] Zhang Z. and Chen Q. *Comparison of the Eulerian and Lagrangian methods for predicting particle transport in enclosed spaces* ACER - Purdue University, 2007.

[54] Zikanov, O. *Essential computational fluid dynamics* Wiley, 2010.